JCI The Journal of Clinical Investigation

# Neddylation stabilizes $Na_V1.1$ to maintain interneuron excitability and prevent seizures in murine epilepsy models

Wenbing Chen, … , Wen-Cheng Xiong, Lin Mei

*J Clin Invest.* 2021;131(8):e136956. https://doi.org/10.1172/JCI136956.

Research Article Neuroscience

## Graphical abstract

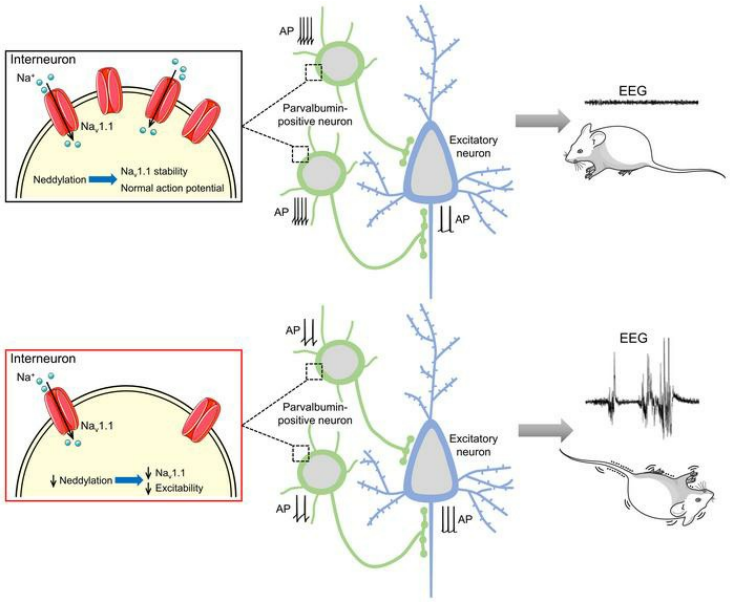

# Neddylation stabilizes $Na_v1.1$ to maintain interneuron excitability and prevent seizures in murine epilepsy models

Wenbing Chen,[1] Bin Luo,[1] Nannan Gao,[1] Haiwen Li,[1] Hongsheng Wang,[1] Lei Li,[1,2] Wanpeng Cui,[1] Lei Zhang,[1] Dong Sun,[1] Fang Liu,[3] Zhaoqi Dong,[1] Xiao Ren,[1] Hongsheng Zhang,[1] Huabo Su,[3] Wen-Cheng Xiong,[1,4] and Lin Mei[1,4]

[1]Department of Neurosciences, School of Medicine, Case Western Reserve University, Cleveland, Ohio, USA. [2]School of Life Science and Technology, ShanghaiTech University, Shanghai, China. [3]Medical College of Georgia, Augusta University, Augusta, Georgia, USA. [4]Louis Stokes Cleveland Veterans Affairs Medical Center, Cleveland, Ohio, USA.

**The excitability of interneurons requires $Na_v1.1$, the α subunit of the voltage-gated sodium channel. $Na_v1.1$ deficiency and mutations reduce interneuron excitability, a major pathological mechanism for epilepsy syndromes. However, the regulatory mechanisms of $Na_v1.1$ expression remain unclear. Here, we provide evidence that neddylation is critical to $Na_v1.1$ stability. Mutant mice lacking Nae1, an obligatory component of the E1 ligase for neddylation, in parvalbumin-positive interneurons (PVINs) exhibited spontaneous epileptic seizures and premature death. Electrophysiological studies indicate that Nae1 deletion reduced PVIN excitability and GABA release and consequently increased the network excitability of pyramidal neurons (PyNs). Further analysis revealed a reduction in sodium-current density, not a change in channel property, in mutant PVINs and decreased $Na_v1.1$ protein levels. These results suggest that insufficient neddylation in PVINs reduces $Na_v1.1$ stability and thus the excitability of PVINs; the ensuing increased PyN activity causes seizures in mice. Consistently, $Na_v1.1$ was found reduced by proteomic analysis that revealed abnormality in synapses and metabolic pathways. Our findings describe a role of neddylation in maintaining $Na_v1.1$ stability for PVIN excitability and reveal what we believe is a new mechanism in the pathogenesis of epilepsy.**

## Introduction

In the CNS, proper neural activities between excitatory pyramidal neurons (PyNs) and inhibitory interneurons (INs) are critical to brain function. In particular, parvalbumin-positive ($PV^+$) interneurons (PVINs) are a major source of inhibitory signal in maintaining excitation-inhibition (E-I) balance. PVINs fire at high frequency and, via feedback and feedforward inhibitions, are necessary for the generation of local circuit oscillations and connectivities or synchronization between brain regions (1–6).The excitability of PVINs requires $Na_v1.1$, the α subunit of voltage-gated sodium channel that is specifically expressed in PVINs (7–13). $Na_v1.1$ deficiency reduces PVIN excitability, increases the threshold of action potential (AP), and decreases AP amplitudes (7, 8, 12, 14–16). On the other hand, PVINs are controlled by a heterogeneous group of voltage-gated potassium channels (such as $K_v3.1$, $K_v3.2$, $K_v3.3$, and KCNQ2/3) whose mutations also change their excitability (17–19). In accordance with this, mutations in $Na_v1.1$ channels have been identified in patients with mild as well as severe forms of epilepsy, including severe myoclonic epilepsy of infancy (SMEI or Dravet syndrome) as well as those with generalized epilepsy with febrile seizures plus ($GEFS^+$) (20–22). Studies of mouse models with $Na_v1.1$ mutations or deletions suggest that epilepsy may be caused by impaired firing of GABAergic INs (7, 12, 16, 23–25). A unified loss-of-function hypothesis posits that mild impairment of $Na_v1.1$ functions causes febrile seizures, intermediate loss-of-function gives rise to $GEFS^+$ epilepsy, and severe impairment causes the intractable seizures and comorbidities of SMEI (26). However, in contrast with the impact of $Na_v1.1$ mutations on channel properties, less is known about mechanisms in regulating $Na_v1.1$'s stability or expression. Nevertheless, mutations could be pathogenic via reducing surface expression caused by aberrant folding, trafficking, or degradation (27, 28).

Neddylation is a chemical reaction in which the ubiquitin-like protein neural precursor cell expressed, developmentally downregulated 8 (Nedd8) is conjugated to the lysine of substrate proteins by its C-terminal glycine (29). Like ubiquitination, neddylation requires Nedd8-specific E1, a heterodimer of NAE1 (also known as APP-BP1) and UBA3, which together activate NEDD8 in an ATP-dependent manner, UBC12 (a Nedd8 E2 enzyme), and substrate-specific E3 ligases. Neddylated proteins could be deneddylated by NEDD8-specific proteases, such as the COP9 signalosome (CSN) and NEDP1 (also known as SENP8; ref. 30). Nedd8 is evolutionarily highly conserved and ubiquitously expressed in many cell types (31, 32). Neddylation regulates a variety of cellular processes, including gene transcription, cell division and differentiation, ribosome biogenesis, apoptosis, and proteolysis (33–35). However, the function of neddylation in the brain is less clear, although it has been recently

▶ Related Commentary: https://doi.org/10.1172/JCI148370

**Authorship note:** W Chen, BL, and NG contributed equally to this work.
**Conflict of interest:** The authors have declared that no conflict of interest exists.

**Submitted:** February 3, 2020; **Accepted:** February 23, 2021; **Published:** April 15, 2021.
**Reference information:** *J Clin Invest*. 2021;131(8):e136956.
https://doi.org/10.1172/JCI136956.

implicated in the development of the neuromuscular junction and excitatory synapses onto PyNs (36, 37).

In this study, we determined whether the development and function of INs is regulated by neddylation. To this end, we mutated NAE1, an obligatory subunit of the only identified Nedd8 E1 enzyme, specifically in PVINs. Unexpectedly, mutant (mt) mice displayed spontaneous epileptic seizures, impaired inhibitory synaptic transmission, and decreased excitability. Yet morphological studies suggest that the mutation had no apparent effect on the number of PVINs in the cortex and hippocampus. Remarkably, the release of GABA, but not glutamate, was reduced in mt mice, which was associated with reduced excitability of PVINs, suggesting that neddylation is critical to controlling the excitability of INs. Further molecular mechanistic studies identified $Na_v1.1$ as a target of Nae1 mutation, which becomes unstable in the absence of neddylation. This notion was supported by proteomic analysis, which also reveals abnormality in synapses and metabolic pathways. Finally, elevated PVIN excitability was attenuated by rescue expression of $Na_v1.1$ in Nae1 mt mice. Together, the results demonstrate a role of neddylation for $Na_v1.1$ stability and GABAergic transmission.

## Results

*Ataxia and spontaneous epileptic seizures in PV-specific Nae1-deficient mice*. To investigate the potential role of neddylation in PVINs, we crossed floxed *Nae1* mice (38) with *PV-Cre* mice in which Cre expression was under the control of the PV promoter (ref. 39 and Figure 1A). NAE1 expression in the brain *of PV-Nae1*$^{-/-}$ mice was characterized. Quantitative real-time PCR (RT-PCR) and Western blot (WB) analyses of hippocampal tissues showed a trend of reduction of NAE1 mRNA and protein between *PV-Nae1*$^{-/-}$ and *PV-Cre* mice, but the reduction was statistically insignificant (Supplemental Figure 1, A–C; supplemental material available online with this article; https://doi.org/10.1172/JCI136956DS1). This was not unexpected because NAE1 is expressed in many types of cells in the brain, including PyN and astrocytes. In accordance with this, immunostaining indicated that NAE1 was reduced in PVINs of hippocampal sections, while no change was observed in PV-negative cells (Figure 1B), suggesting that NAE1 was specifically reduced in PVINs. To test this notion further, cortical neurons were cultured from *PV-Cre::Ai9* mice (referred to as *PV-Ai9*), where tdTomato was specifically expressed in PVINs (40). NAE1 was detectable in PV-positive cells from *PV-Ai9* mice, but not those from *PV-Nae1*$^{-/-}$*-Ai9* mice. NAE1 was also detectable in PV-negative cells, but at similar levels between the 2 genotypes (Supplemental Figure 1, D and E). Together, these results demonstrate that NAE1 was specifically ablated in PVINs in *PV-Nae1*$^{-/-}$ mice. *PV-Nae1*$^{-/-}$ mice showed no difference in brain size and gross cortical morphology, including the thickness and the number of neurons in the somatosensory cortex, compared with *PV-Cre* mice (Supplemental Figure 2).

*PV-Nae1*$^{-/-}$ mice exhibited signs of ataxia and seizure in a development-dependent manner. Beginning on P18, they showed limb tremors and imbalanced or uncoordinated walking or stumbling (Supplemental Video 1). None of these phenotypes were observed in control *PV-Cre* mice at any ages. We assessed ataxia phenotypes by behavioral tests. As shown in Supplemental Figure 3, A–C, in the balance beam test, the latency and distance walked prior to falling from the beam were reduced in *PV-Nae1*$^{-/-}$ mice compared with that in control *PV-Cre* mice (latency: 14.5 ± 6.9 s in mt versus 60.0 ± 0.0 s in control, $P < 0.0001$; distance walked: 9.1 ± 1.6 cm in mt versus 122.8 ± 13.2 cm in control, $P < 0.0001$; $n = 8$ mice per genotype). To assess the motor reflex, mice were tail suspended above a wire lid of a cage, as described previously (ref. 41, see also Methods). Control mice would outstretch forelimbs to reach downward for the cage lid (Supplemental Figure 3D). However, *PV-Nae1*$^{-/-}$ mice displayed a curved body posture and seemingly were unable to reach for the lid. The reflex response time was reduced in mt mice compared with control mice (Supplemental Figure 3E; 29.7% ± 4.09% in mt versus 96.8% ± 1.33% in control, $P < 0.0001$; $n = 8$ mice per genotype). These results indicate that the Nae1 mutation in PVINs causes ataxia-like phenotypes in mice. *PV-Nae1*$^{-/-}$ mice began to display epileptic seizures around P30 (Supplemental Video 2), which were associated with epileptiform discharges by EEG recording (Figure 1C). At P40, 1 seizure onset was observed every 4 hours (Figure 1D), and the frequency and severity of seizures were increased with age. At P47, *PV-Nae1*$^{-/-}$ mice began to die, which resulted from a general seizure or sudden unexpected death in epilepsy (Figure 1E). These results demonstrate a critical role of NAE1 of PVIN in regulating brain activity.

*A necessary role of Nae1 for PVIN excitability*. To investigate the underlying mechanisms, we quantified the number of PVINs in *PV-Nae1*$^{-/-}$ mice in the hippocampus, but failed to detect any difference between the mt and control mice (Figure 1, F–J). Similar results were observed in the medial prefrontal cortex (mPFC) and amygdala (Supplemental Figure 4). Next, we recorded spontaneous excitatory postsynaptic currents (sEPSCs) in CA1 PyNs in whole-cell patch configurations without blocking glutamatergic and GABAergic transmission. Interestingly, the frequency of sEPSC in CA1 PyNs was increased without altered amplitude (Figure 2, A–C; sEPSC frequency, 2.64 ± 0.30 Hz in mt versus 1.66 ± 0.32 Hz in control, $P < 0.05$; sEPSC amplitude 19.17 ± 0.99 pA in mt versus 18.60 ± 0.65 pA in control, $P = 0.6372$; $n = 9$ neurons from 3 mice per genotype), indicating increased PyN activity in mt mice. To determine whether this was due to altered function of PVINs or PyNs, we next measured spontaneous inhibitory postsynaptic currents (sIPSCs) of CA1 PyNs in the presence of 6-cyano-7-nitroquinoxaline-2,3-dione (CNQX) and DL-2-amino-5-phosphonopentanoic acid (DL-AP5) (antagonists of AMPA receptors and NMDA receptors, respectively) to block glutamatergic transmission. As shown in Figure 2, D and E, sIPSC frequency was reduced in *PV-Nae1*$^{-/-}$ mice compared with that in *PV-Cre* mice (sIPSC frequency, 6.92 ± 0.93 Hz in mt versus 11.39 ± 1.16 Hz in control, $P < 0.01$; $n = 12$ neurons from 4 control mice; $n = 11$ neurons from 4 mt mice). However, Nae1 mutation had little effect on sIPSC amplitudes (Figure 2F; sIPSC amplitude, 43.4 ± 4.36 pA in mt versus 39.9 ± 2.70 pA in control, $P = 0.503$). These results suggest that the Nae1 mutation may decrease GABAergic transmission from PVINs onto PyNs in the hippocampus. Next, we recorded sEPSCs when GABAergic transmission was blocked by bicuculline (an antagonist of GABAA receptors), but failed to detect any difference in sEPSC frequency or amplitudes (Figure 2, G–I; sEPSC frequency, 1.49 ± 0.18 Hz in mt versus 1.48 ± 0.16 Hz in control, $P = 0.9501$; sEPSC amplitude, 17.7 ± 1.00 pA in mt versus 16.5 ± 0.71 pA in control, $P = 0.3407$; $n = 11$ neurons from 4 mice per genotype). These observations indicate that the increase in sEPSC is likely caused by reduced GABA release from PVINs.

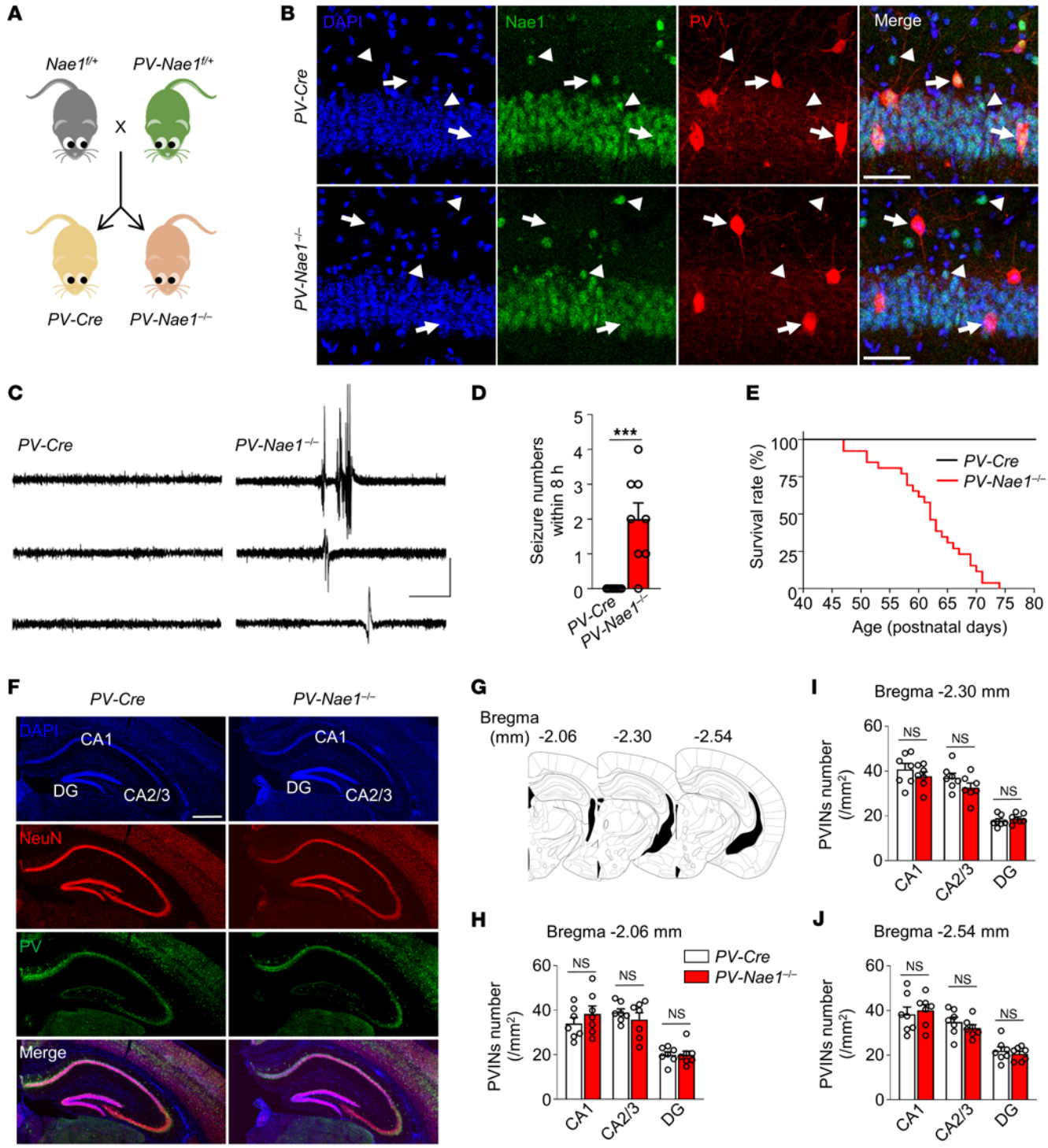


**Figure 1. Spontaneous seizures and premature death in Nae1-deficient mice**. (**A**) Schematic diagram of breeding strategy to generate *PV-Nae1*$^{-/-}$ and *PV-Cre* mice. (**B**) Specific ablation of Nae1 in PVINs. Hippocampus sections of *PV-Cre* (top) and *PV-Nae1*$^{-/-}$ (bottom) mice were stained with anti-Nae1 (green) and anti-PV (red) antibodies. Nuclei are shown in blue (DAPI staining). Arrows show PV-positive cells, and arrowheads show PV-negative cells. Scale bar: 50 μm. $n$ = 3 experiments. (**C**) Representative EEG traces of freely moving *PV-Cre* and *PV-Nae1*$^{-/-}$ mice. Scale bar: 20 s, 2 mV. (**D**) Quantitative analysis of seizure numbers within 8 hours. $n$ = 8 mice for each genotype. *PV-Cre* (0 ± 0 seizure numbers) vs. *PV-Nae1*$^{-/-}$ (2 ± 0.46 seizure numbers). $P < 0.001$. (**E**) Survival curves of *PV-Cre* ($n$ = 28) and *PV-Nae1*$^{-/-}$ ($n$ = 26) mice. (**F**–**J**) No change in PVIN number in hippocampus of *PV-Nae1*$^{-/-}$ mice. (**F**) Fluorescence images showing the PVINs in the hippocampus. Scale bar: 500 μm. (**G**) Schematic representation of coronal sections of the hippocampus. Numbers indicate distance from bregma. (**H**–**J**) Quantification of PVINs in CA1, CA2/3, and DG regions of the 3 coronal sections. $n$ = 7 slices, 3 mice for each genotype. Slices were stained with anti-NeuN (red) and PV (green) antibodies; nuclei are shown in blue (DAPI staining). Data are represented as mean ± SEM. ***$P < 0.001$, unpaired 2-tailed Student's $t$ test.

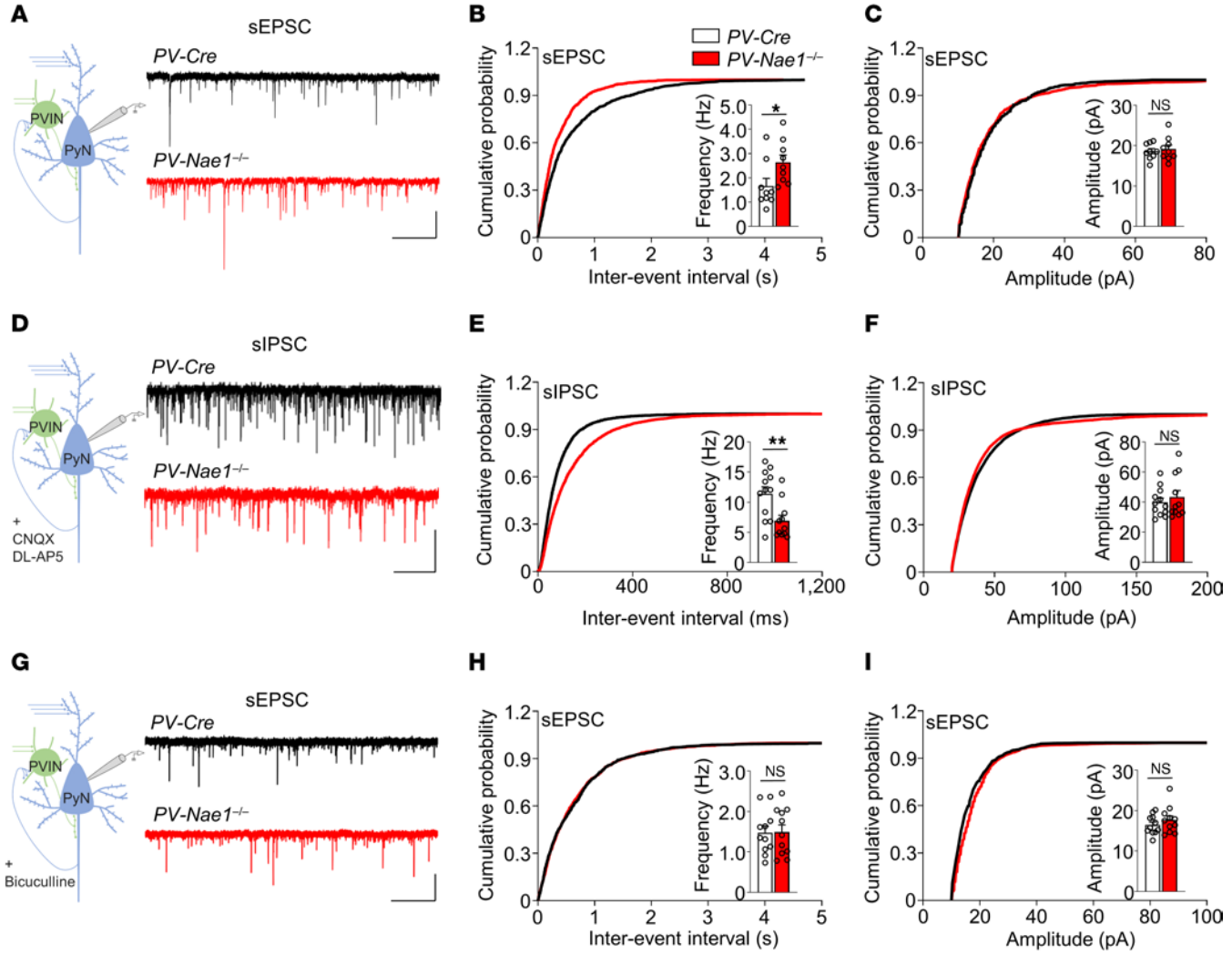


**Figure 2. Reduced GABAergic neurotransmission in *PV-Nae1*$^{-/-}$ hippocampus**. (**A**) Representative sEPSC traces of CA1 PyNs without blocking GABAergic and glutamatergic transmission. Left, schematic diagram of recording. Scale bar: 3 s, 40 pA. (**B**) Increased sEPSC frequency. *n* = 9 neurons, 3 mice for each genotype. (**C**) No difference in sEPSC amplitudes. (**D**) Representative sIPSC traces of CA1 PyNs with blocking glutamatergic transmission (right). Left, schematic diagram of recording. Scale bar: 1 s, 50 pA. (**E**) Decreased sIPSC frequency. *n* = 11–12 neurons, 4 mice for each genotype. (**F**) No difference in sIPSC amplitudes. (**G**) Representative sEPSC traces of CA1 PyNs with blocking GABAergic transmission (right). Left, schematic diagram of recording. Scale bar: 3 s, 40 pA. (**H**) No difference in sEPSC frequency. *n* = 11 neurons, 4 mice for each genotype. (**I**) No difference in sEPSC amplitudes. Data are represented as mean ± SEM. **P* < 0.05; ***P* < 0.01, unpaired 2-tailed Student's *t* test.

To investigate the mechanisms of reduced GABA release in *PV-Nae1*$^{-/-}$ mice, we examined the intrinsic excitability of CA1 PVINs by clamping in a whole-cell configuration. APs of PVINs were elicited by injecting depolarizing currents at different intensities in the presence of bicuculline, CNQX, and DL-AP5 to block both inhibitory and excitatory neurotransmission. Intriguingly, the firing frequency of PVINs in response to depolarizing currents was lower in *PV-Nae1*$^{-/-}$*-Ai9* mice compared with *PV-Ai9* mice (Figure 3, A and B; gene effect, $F_{1,196} = 34.36$, $P < 0.0001$; interaction effect, $F_{6,196} = 3.15$, $P < 0.01$; 2-way ANOVA). A similar reduction in PVIN firing frequency was observed in the mPFC and amygdala of *PV-Nae1*$^{-/-}$*-Ai9* mice (Supplemental Figure 5). In contrast, there was no difference in the resting membrane potential (RMP), membrane capacitance ($C_m$), and input resistance ($R_{in}$) of PVINs between *PV-Ai9* and *PV-Nae1*$^{-/-}$*-Ai9* mice (Figure 3, C–E). Importantly, the firing frequency of PyNs in the presence of bicuculline, CNQX, and DL-AP5 was similar between the 2 genotypes (Figure 3, F and G; gene effect, $F_{1,168} = 0.2578$, $P = 0.6123$; interaction effect, $F_{6,168} = 0.158$, $P = 0.9872$; 2-way ANOVA). Moreover, no difference was observed in passive membrane properties of PyNs (Figure 3, H–J), including RMP, $C_m$, and $R_{in}$ of PyNs between *PV-Ai9* and *PV-Nae1*$^{-/-}$*-Ai9* mice. However, in the absence of glutamatergic and GABAergic transmission blockers, PyN firing was increased in *PV-Nae1*$^{-/-}$*-Ai9* mice compared with controls (Figure 3, K and L; gene effect, $F_{1,119} = 27.52$, $P < 0.0001$; interaction effect, $F_{6,119} = 2.568$, $P < 0.05$; 2-way ANOVA). Together, these results indicate that Nae1 deletion in PVINs reduces the intrinsic excitability of PVINs, but not that of PyNs. The resulting reduced GABA release subsequently led to increased PyN firing and glutamatergic transmission. The effect of Nae1 mutation on PVINs was specific because it had little effect on the excitability of cholecystokinin-positive INs (CCKINs) (Supplemental Figure 6, A–C) or

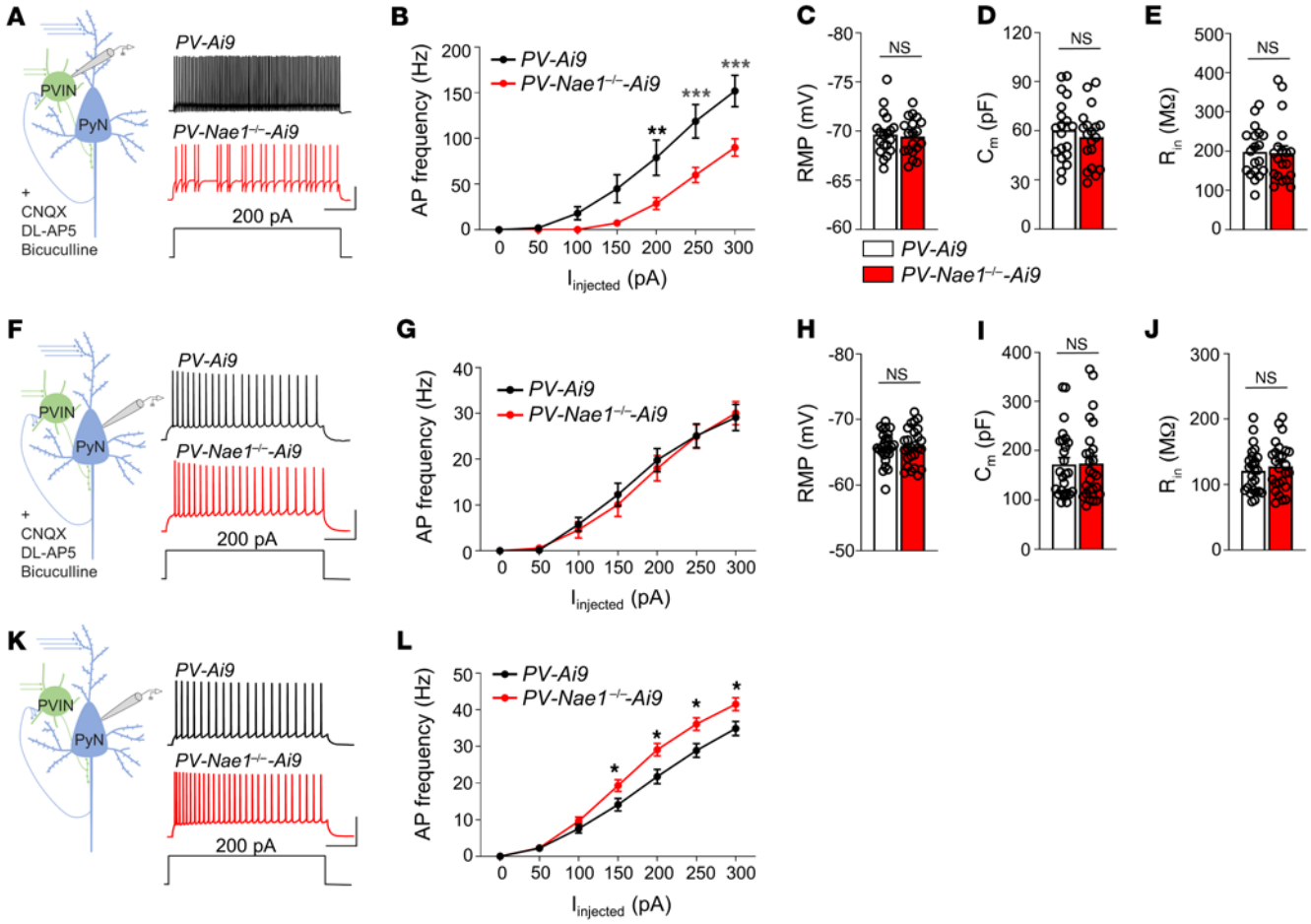


**Figure 3. Impaired PVIN intrinsic excitability in *PV-Nae1*–deficient mice**. (**A** and **B**) Impaired PVIN intrinsic excitability of *PV-Nae1*–deficient mice with blocking glutamatergic and GABAergic transmissions. Schematic diagram of recording (left in **A**) and representative AP traces (right in **A**). Quantification of current injection–induced APs in PVINs (**B**). $n$ = 15 neurons, 4 mice for each genotype. Scale bar: 0.2 s, 30 mV. (**C**–**E**) No difference in RMP (**C**), $C_m$ (**D**), or $R_{in}$ (**E**) in PVINs between the 2 groups. $n$ = 19 neurons, 4 mice for each genotype. (**F** and **G**) No change in PyN intrinsic excitability in CA1 of *PV-Nae1*–deficient mice. Schematic diagram of recording (left in **F**) and representative AP traces (right in **F**). Quantification of current injection–induced APs in PyNs (**G**). $n$ = 12–14 neurons, 4 mice for each genotype. Scale bar: 0.2 s, 40 mV. (**H**–**J**) No difference in RMP (**H**), $C_m$ (**I**), or $R_{in}$ (**J**) in CA1 PyNs between the 2 groups. $n$ = 26 neurons, 4 mice for each genotype. (**K** and **L**) Increased PyN network excitability in CA1 of *PV-Nae1*–deficient mice. Schematic diagram of recording (left in **K**) and representative AP traces (right in **K**). Quantification of current injection–induced APs (**L**) in PyNs. $n$ = 9–10 neurons, 3 mice for each genotype; Scale bar: 0.2 s, 40 mV. Data are represented as mean ± SEM. $^*P < 0.05$; $^{**}P < 0.01$; $^{***}P < 0.001$, unpaired 2-tailed Student's $t$ test (**C**, **D**, **E**, **H**, **I**, and **J**); 2-way ANOVA (**B**, **G**, and **L**).

the RMP and current-voltage relationship of astrocytes that may regulate neuronal activity (Supplemental Figure 6, D–H).

*Sodium-current deficiency to decrease PVIN excitability in PV-Nae1$^{-/-}$-Ai9 mice*. The excitability of PVINs is regulated by many proteins, including neural proteoglycan brevican (BCAN), ETS variant transcription factor 1 (ER81), and various ion channels. including hyperpolarization-activated cyclic nucleotide-gated potassium channel 4 (HCN4), voltage-gated potassium channels (KCNA1, KCNC1-3, KCNQ2, and KCNQ3), and the α subunits of voltage-gated sodium channel (SCN1A, SCN3A, and SCN8A, refs. 7, 8, 12, 17–19, 42–45). To investigate how Nae1 mutation regulates PVIN excitability, we analyzed the mRNA levels of these genes by quantitative RT-PCR analyses; no differences were observed between *PV-Ai9* and *PV-Nae1$^{-/-}$-Ai9* mice, suggesting that Nae1 mutation in PVINs did not alter these proteins' synthesis transcription (Supplemental Figure 7A).

To reveal the mechanisms underlying decreased PVIN excitability, we analyzed the APs elicited in response to individual injection of 400 pA depolarizing current ramp in tdTomato$^+$ INs (Figure 4A). APs of these INs had a large and rapid afterhyperpolarization (AHP) phase (Figure 4B), as previously reported for PVINs (46, 47). Compared with control PVINs, rheobase (the minimal current to trigger the first AP) was increased in Nae1 mt PVINs (Figure 4C, rheobase, 193.3 ± 17.7 pA in mt versus 128.9 ± 12.0 pA in control, $P < 0.01$), consistent with reduced excitability in mt PVINs. To determine which channels may be altered by Nae1 mutation, we measured AP threshold (membrane potential to generate AP) and amplitude, the 2 events dependent on voltage-gated sodium channels ($Na_v$; refs. 48–51). As shown in Figure 4D, AP thresholds were increased (less negative) in mt PVINs compared with those in controls (threshold, –40.4 ± 1.12 mV in mt versus –44.4 ± 1.15 mV in control, $P < 0.05$; $n$ = 19 neurons from 4 mice per genotype). AP amplitudes were reduced in PVINs of Nae1 mt mice compared with those in control mice (Figure 4E; amplitude, 49.6 ± 1.88 mV in mt versus 56.3 ± 1.60 mV in control, $P < 0.05$). These results suggest a deficiency of $Na_v$ in Nae1 mt

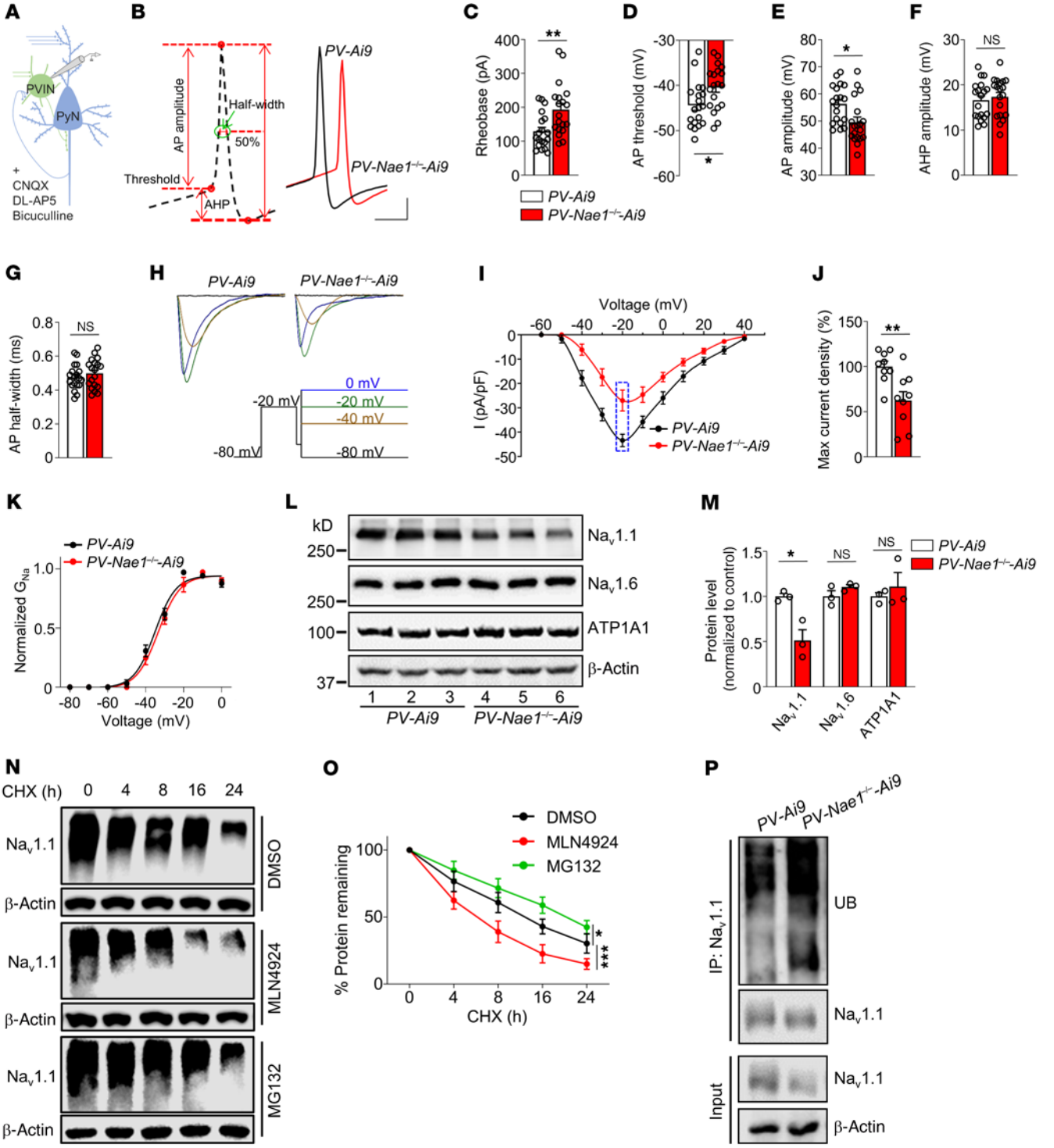


**Figure 4. Decreased Na current density and reduced $Na_v1.1$ level and stability in *PV-Nae1*–deficient mice.** (**A** and **B**) Schematic diagram of recording (**A**) and representative second AP waveform in CA1 PVINs evoked by a 400 pA ramp current injection (**B**). Scale bar: 2 ms, 10 mV. (**C**–**G**) Increased rheobase (**C**) and AP threshold (**D**). Decreased AP amplitude (**E**). No changed AHP amplitude (**F**) and AP half-width (**G**). $n$ = 19 neurons, 4 mice for each genotype. (**H**) Representative traces of voltage-gated sodium currents in CA1 PVINs. Scale bar: 5 ms, 5 pA/pF. (**I**) Current-voltage curves. $n$ = 9 neurons, 4 mice for each genotype. (**J**) Reduction of the maximum sodium-current density in *PV-Nae1*$^{-/-}$*-Ai9* mice. (**K**) Comparison of the voltage-dependence activation of sodium channels. Conductance was normalized to the maximal sodium conductance; lines were generated by Boltzmann fitting. Membrane potentials for half-maximal activation and slope factors were as follow: *PV-Ai9*, -35.10 ± 0.77 mV and 5.51 ± 0.66; *PV-Nae1*$^{-/-}$*-Ai9*, –33.38 ± 0.87 mV and 5.75 ± 0.76. (**L** and **M**) Levels of $Na_v1.1$ protein were lower in *PV-Nae1*$^{-/-}$*-Ai9* mice. (**L**) Representative blots for hippocampal tissues. (**M**) Quantification analysis of data. (**N** and **O**) Accelerated $Na_v1.1$ degradation by neddylation inhibition. (**N**) tsA-201 cells were cotransfected with human $Na_v1.1$ channel $\beta_1$ and $\beta_2$ subunits, treated with DMSO, MLN4924, or MG132. (**O**) Quantification analysis of data. $n$ = 4 experiments. (**P**) Increased ubiquitinated $Na_v1.1$ in *PV-Nae1*$^{-/-}$*-Ai9* mice. Cerebellar lysates were subjected to immunoprecipitation with anti-$Na_v1.1$ antibody and immunoblotting with anti-UB (K48) antibody. $n$ = 3 experiments. Data are represented as mean ± SEM. *$P$ < 0.05; **$P$ < 0.01; ***$P$ < 0.001, unpaired 2-tailed Student's $t$ test (**C**, **D**, **E**, **F**, **G**, **J**, and **M**); 2-way ANOVA (**O**).

PVINs. Notice that the effects of Nae1 mutation on sodium channels were specific because the mutation had little effect on AHP amplitudes, which require $Ca^{2+}$-activated voltage-dependent $K^+$ channels (Figure 4F; 17.4 ± 0.98 mV in mt versus 16.6 ± 0.93 mV in control, $P$ = 0.5839). Nae1 mutation had no effect on the AP half-widths (Figure 4G; 0.50 ± 0.02 ms in mt versus 0.48 ± 0.02 ms in control, $P$ = 0.3744), suggesting voltage-gated potassium channels and calcium channels might not be affected (51–53). These results indicate that Nae1 mutation increased rheobase and thresholds to generate APs in PVINs, suggesting the deficient $Na_v$ as a potential mechanism (16).

To further test this idea, we analyzed somatic $Na^+$ currents in CA1 PVINs by using a prepulse protocol (ref. 54 and Figure 4H). The $Na^+$ currents could be completely abolished by tetrodotoxin, a specific blocker of sodium channels (data not shown). Voltage-clamp step recording showed that the $Na_v$ current density (normalized by cell capacitance) was reduced in *PV-Nae1$^{-/-}$-Ai9* mice compared with that in *PV-Ai9* mice (Figure 4, I and J; max current density 62.3% ± 9.92% in mt versus 100% ± 5.89% in control, $P < 0.01$; $n = 9$ neurons from 4 mice per genotype). Nae1 mutation had little effect on voltage-gated calcium currents or hyperpolarization-activated cyclic nucleotide-gated channel currents in PVINs (Supplemental Figure 7, B–F). Notice that the voltage dependence of activation for $Na^+$ currents was not changed (Figure 4K), suggesting that mt PVINs have normal $Na_v$ electrophysiological properties. These results suggest that Nae1 mutation reduced $Na_v$ currents without changing $Na_v$'s properties.

*A necessary role of neddylation for $Na_v1.1$ stability*. In the mammalian CNS, $Na_v1.1$, and $Na_v1.6$ are abundant in PVINs, whereas $Na_v1.2$ is mainly expressed in excitatory neurons. $Na_v1.3$ is transiently expressed in the brain during embryonic development and normally absent in the adult (7, 11, 55). To determine whether $Na_v1.1$ protein was reduced in PVINs of *PV-Nae1$^{-/-}$-Ai9* mice, we did WB analysis. As shown in Figure 4, L and M, $Na_v1.1$, but not $Na_v1.6$ and Atp1a1 ($Na^+/K^+$-ATPase α 1 subunit), were reduced in the hippocampus of *PV-Nae1$^{-/-}$-Ai9* mice. $Na_v1.1$ reduction was also observed in cerebral cortex and cerebellum (Supplemental Figure 8), brain regions where PVINs are abundant. These results support the idea that $Na_v1.1$ reduction may be a potential mechanism for decreased excitability of PVINs. This notion was supported by increased AP failure rate in PVINs of *PV-Nae1$^{-/-}$-Ai9* mice compared with *PV-Ai9* mice (Supplemental Figure 9). These electrophysiologic deficits, as well as ataxia and seizure phenotypes (Figure 1 and Supplemental Figure 3), were similar to those of $Na_v1.1$ mt mice (7, 8, 12, 16, 41). Together, these results suggest $Na_v1.1$ deficiency as a pathology mechanism.

Next, we investigated the molecular mechanisms underlying $Na_v1.1$ protein reduction in *PV-Nae1$^{-/-}$-Ai9* mice. As shown in Supplemental Figure 6A, $Na_v1.1$ mRNA levels were similar between the genotypes. Because neddylation is known to regulate protein stability (56–58), we wondered whether $Na_v1.1$ stability requires neddylation. To this end, h$Na_v1.1$ and 2 β subunits were transfected into human tsA-201 cells, SV40-transformed HEK293 cell that are able to express ion channels on the membrane (59). Forty-eight hours after transfection, cells were incubated with 50 μM cycloheximide (CHX) to inhibit protein synthesis and with MLN-4924, a potent and selective inhibitor of NAE (60, 61). Interestingly, $Na_v1.1$ degradation was increased in MLN-4928–treated cells compared with nontreated cells (Figure 4, N and O), suggesting a critical role of neddylation for $Na_v1.1$ stability. In accordance with this, K48-linked ubiquitination was increased in *PV-Nae1$^{-/-}$-Ai9* mice compared with *PV-Ai9* mice (Figure 4P). These results suggest that neddylation may be critical to the stability of $Na_v1.1$.

*Neddylation-dependent surface expression of $Na_v1.1$*. To determine whether $Na_v1.1$ is subjected to modification by neddylation, we transfected tsA-201 cells with $Na_v1.1$-Myc together with HA-Nedd8. $Na_v1.1$ was immunoprecipitated by anti-Myc antibody and probed with anti-HA antibody. Interestingly, HA signal was detected in precipitated $Na_v1.1$; importantly, the signal was reduced in cells that were incubated with the NAE inhibitor MLN-4924 (Figure 5A). These results suggest that the channel may be neddylated in tsA-201 cells. To determine whether $Na_v1.1$ neddylation occurs in vivo, $Na_v1.1$ was precipitated with anti-$Na_v1.1$ antibody from cerebellar homogenates (where $PV^+$ cells are abundant) and probed with anti-Nedd8 antibody, as previously described (36, 62). Neddylated $Na_v1.1$ was reduced in *PV-Nae1*–deficient mice compared with control mice (Figure 5B). Together, these results demonstrate that $Na_v1.1$ is neddylated in cultured cells and in the brain.

To further investigate how neddylation regulates $Na_v1.1$, we sought to identify the lysine residues in $Na_v1.1$ that may be subjected to neddylation. We screened for potential pathogenic lysine mutations in databases of epilepsy patients and the ClinVar in the US National Library of Medicine. Sixteen lysine missense mutations were reported in patients with epilepsy (63–69); in particular, K1936E (where lysine1936 was mutated to glutamic acid) was identified in a screen of 70 genes in 8565 patients, including 8354 epileptic patients (68) (see also Human SCN1A gene database; http://scn1a.caae.org.cn/index.php). Because K1936 is localized in the cytoplasmic region of $Na_v1.1$, we determined whether its mutation alters the stability of the $Na_v1.1$ protein. WT-$Na_v1.1$ or K1936E, along with 2 β subunits, was transfected into tsA-201 cells, and their stability was studied in the presence of CHX. Compared with WT-$Na_v1.1$, K1936E was degraded faster (Figure 5, C and D). As a control, the stability was not changed for K245N, another lysine mutation also located in the cytoplasmic domain. In agreement with this, surface and total levels of K1936E, but not K245N, were reduced (Figure 5, E–G). Concomitantly, $Na_v1.1$ neddylation was reduced in cells expressing K1936E, but not K245N, indicating that Lys1936 is a primary neddylation site (Figure 5, H and I). These results suggest that neddylation at Lys1936 is important in maintaining the stability of $Na_v1.1$ and that K1936E mt is less stable, identifying a potential pathological mechanism of this mutation.

To investigate whether the functional properties of $Na_v1.1$ channels were changed by these mutations, tsA-201 cells were transfected with WT-$Na_v1.1$, K245N, or K1936E, together with $\beta_1$ and $\beta_2$ subunits and GFP (70), and were recorded by patch clamp in whole-cell configuration. The current-voltage curves showed that the current density was reduced in cells expressing K1936E, but not K245N, compared with WT (Figure 6, A and B). Notice that the coprecipitation of mt $Na_v1.1$ and $\beta_1$ or $\beta_2$ subunits was comparable to that of WT-$Na_v1.1$, suggesting that the K1936E mutation had no impact on $Na_v1.1$ interaction with $\beta_1$ or $\beta_2$ subunits (Supplemental Figure 10). Next, we characterized the kinetics of the sodium-channel activation and inactivation. As shown in Figure 6, C and D, the curves of activation and inactivation were similar between WT-$Na_v1.1$ and K1936E, suggesting that the mutation did not change the voltage-dependent activation and inactivation

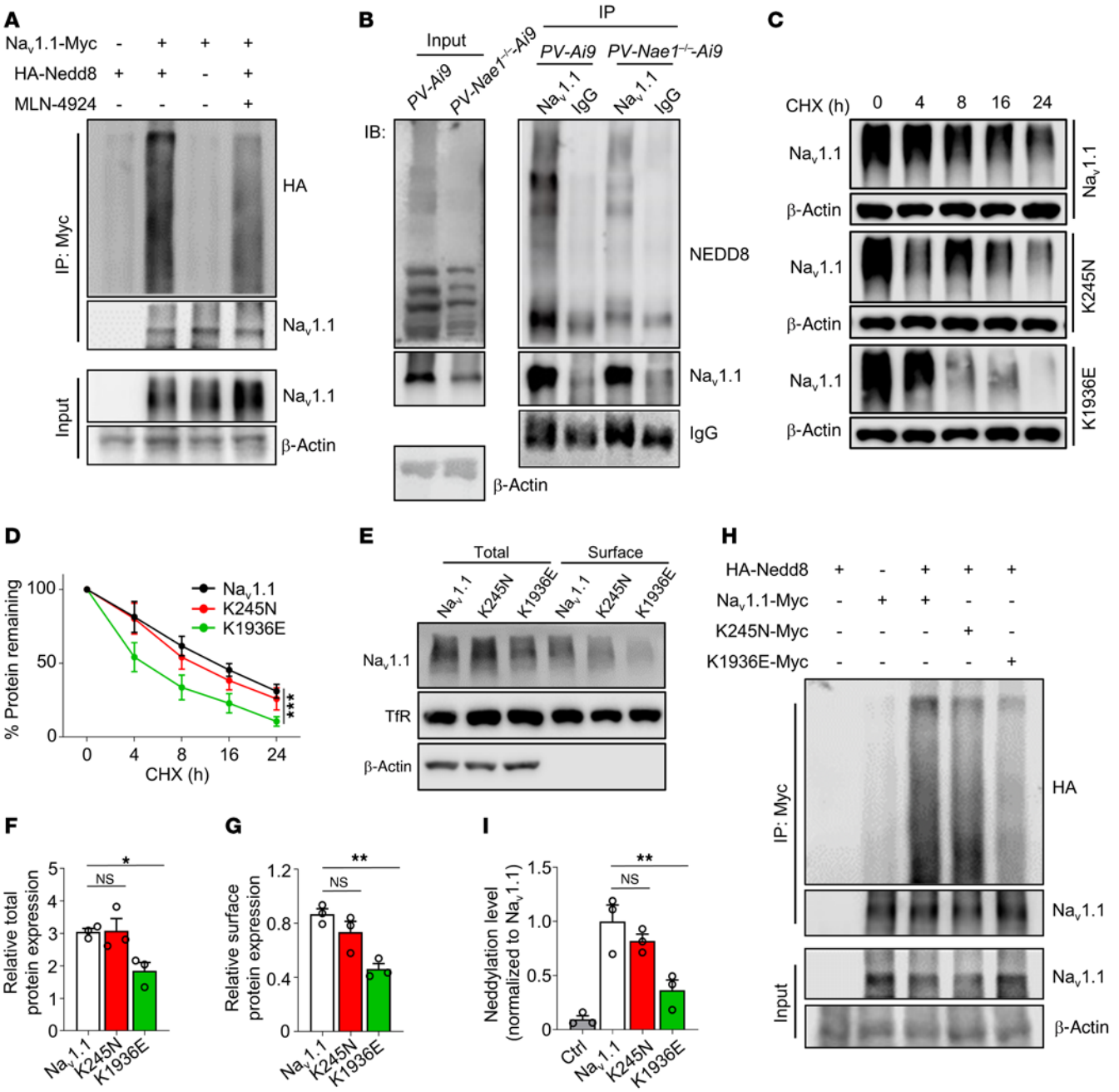


**Figure 5. Reduced surface expression of K1936E mt Na$_v$1.1.** (**A**) Inhibiting Na$_v$1.1 neddylation by MLN4924. tsA-201 cells were transfected with Na$_v$1.1-Myc and HA-Nedd8 plasmids and treated with or without MLN-4924. $n$ = 3 experiments. (**B**) Decreased Na$_v$1.1 neddylation in *PV-Nae1*$^{-/-}$*-Ai9* mice. Neddylated Na$_v$1.1 precipitated with anti-Na$_v$1.1 antibody and probed with anti-NEDD8 antibody. $n$ = 3 experiments. (**C**) Accelerated degradation of K1936E. tsA-201 cells were cotransfected with Na$_v$1.1-WT, K245N or K1936E with $\beta_1$ and $\beta_2$ subunits, treated with CHX for indicated times, and subjected to immunoblotting. $n$ = 3 experiments. (**D**) Quantification analysis of data in **C**. (**E**–**G**) Reduced total and surface K1936E Na$_v$1.1 in tsA-201 cells. Representative blots for tsA-201 cells (**E**), quantitative data of total (**F**) and surface (**G**) levels. $n$ = 3 experiments. (**H** and **I**) Reduced neddylation at K1936E. (**H**) Na$_v$1.1-WT, K245N, and K1936E were transiently transfected in tsA-201 cells together with HA-Nedd8. (**I**) Quantification analysis of data. $n$ = 3 experiments. Data are represented as mean ± SEM. $^*P < 0.05$; $^{**}P < 0.01$; $^{***}P < 0.001$, 1-way ANOVA (**F**, **G**, and **I**); 2-way ANOVA (**D**).

of sodium currents, respectively. In addition, K245N showed a depolarizing shift of steady-state fast inactivation. Together, these results demonstrate that the K1936E mutation reduces Na$_v$1.1 levels without altering the channel property.

*Altered synaptic functions revealed by proteomic analysis*. Sodium-channel levels and function are regulated by a variety of proteins or pathways. For example, increased intracellular calcium concentrations reduced sodium-current density (71). Sodium-channel surface expression and stability require auxiliary β subunits, such as SCN1B and SCN2B (72, 73). Fibroblast growth factor 14 (FGF14) interacts with and inhibits sodium channels (74, 75), whereas loss of FGF14 reduced Na$_v$1.6 expression (76). Finally, neural precursor cell expressed, developmentally downregulated 4 like (NEDD4L), a ubiquitin E3 ligase, decreases the

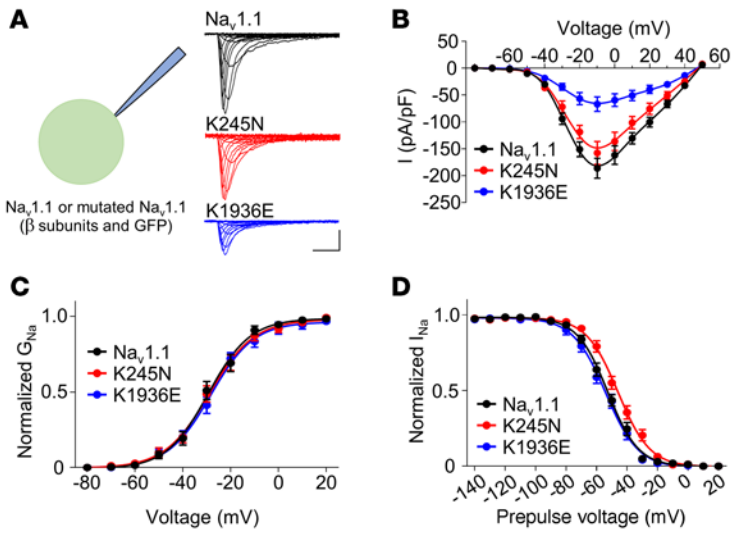


**Figure 6. Reduced Na$_v$ current density by the K1936E mutation**. (**A**) Representative whole-cell sodium currents. tsA-201 cells were injected with depolarizing steps from −80 to +50 mV, with a holding potential of −120 mV. Scale bar: 2 ms, 50 pA/pF. (**B**) Current-voltage relationships. Whole-cell sodium currents were normalized to cell capacitance. *n* = 10–11 cells for each group. Sodium-current density is significantly decreased in K1936E group compared with WT group. (**C**) Comparison of the voltage-dependence activation of sodium channels. Conductance was normalized to the maximal sodium conductance between −80 and +20 mV; lines represent mean Boltzmann fits. *n* = 10–11 cells for each group. The membrane potentials for half-maximal activation and slope factors were as follows: WT, −29.3 ± 0.98 mV and 8.8 ± 0.9; K245N, −29.0 ± 1.05 mV and 9.3 ± 0.97; K1936E, −28.3 ± 1.04 mV and 9.0 ± 0.95. (**D**) Depolarizing shift (+6.8 mV) of steady-state fast inactivation of Na$_v$1.1 with K245N mutation. Currents were normalized to the peak current amplitude; lines represent mean Boltzmann fits. *n* = 10–11 cells for each group. The membrane potentials for half-maximal inactivation and slope factors were as follows: WT, −52.7 ± 0.60 mV and 10.1 ± 0.53; K245N, −45.9 ± 0.66 mV and 10.5 ± 0.59; K1936E, −54.1 ± 0.72 mV and 10.8 ± 0.64. Data are represented as mean ± SEM.

sodium-channel density at cell surface in Xenopus oocytes and heart cells (77–79). Receptor for activated C kinase 1 (RACK1) inhibits mRNA expression of Na$_v$1.1 by binding to a silencer downstream of the SCN1A promoter (80). As shown in Supplemental Figure 11, mRNA levels of these proteins were similar between *PV-Nae1$^{-/-}$-Ai9* mice and *PV-Ai9* mice.

To fully understand the impact of the PVIN-specific Nae1 mutation on brain function, we compared the proteomes between *PV-Nae1$^{-/-}$-Ai9* mice and *PV-Ai9* mice (Figure 7A). Out of a total of 5167 proteins identified (Supplemental Table 1), 169 and 279 proteins were down- and upregulated, respectively, in *PV-Nae1$^{-/-}$-Ai9* mice compared with *PV-Ai9* mice ($P < 0.05$; Figure 7B). As expected, NAE1 was reduced in mt brain samples (Figure 7B), in support of our hypothesis. Gene Ontology (GO) analysis of downregulated proteins implicated a variety of cellular functions (Supplemental Table 2). Interestingly, 9 of the top 20 relate to neural development, neurotransmission, and synaptic plasticity, including dendrite development, synapse organization, synaptic vesicle exocytosis, and glutamatergic transmission (Figure 7C and Supplemental Table 2), in accordance with a previous report (37). In agreement, Kyoto Encyclopedia of Genes and Genomes (KEGG) analysis highlighted glutamatergic and dopaminergic synapses, synaptic vesicle cycle, endocannabinoid signaling, and alcoholism as well as spliceosome (Supplemental Figure 12A and Supplemental Table 3; $P < 0.05$). On the other hand, for upregulated proteins, GO analysis pointed to ubiquitin-regulated catabolism and protein folding and localization (Figure 7D and Supplemental Table 4), whereas KEGG analysis highlighted metabolic pathways, including propanoate, pyruvate and carbon metabolism, tRNA synthesis, phagocytosis, and ubiquitin-mediated proteolysis (Supplemental Figure 12B and Supplemental Table 5, $P < 0.05$). These results suggest that Nae1 is required not only for maintaining the excitability and GABA release of PVINs, but also for a plethora of cellular functions, such as RNA splicing, metabolism, protein processing and stability, and phagocytosis.

Considering compromised intrinsic excitability of PVINs in Nae1 mt mice, we wondered whether the levels of other ion channels are altered. Indeed, among the identified proteins were 53 ion channels (Figure 7E and Supplemental Table 1). However, only SCN1A and voltage-gated calcium channel auxiliary subunit γ 7 (CACNG7) were significantly changed (in fact reduced) in *PV-Nae1$^{-/-}$-Ai9* samples compared with control *PV-Ai9* samples (Figure 7E; $P < 0.05$). CACNG7 is a type II transmembrane AMPA receptor regulatory protein (TARP) that regulates trafficking and channel gating of the AMPA receptors (81); however, CACNG7 mt mice were apparently normal in locomotion and excitatory transmission (81, 82), suggesting that CACNG7 reduction may not contribute to epileptic behavior in Nae1 mt mice. On the other hand, recent studies have identified 29 risk genes for epilepsy (20–22, 83–87) (Figure 7F). Intriguingly, in addition to Na$_v$1.1/SCN1A, GABAA receptor δ subunit (GABRD, a subunit of extrasynaptic GABAA receptor) and proline-rich transmembrane protein 2 (PRRT2, a synaptic protein implicated in synaptic formation and maintenance) were also reduced (Figure 7F). However, IN-specific deletion of GABRD increased IN excitability and thus decreased PyN excitability and seizure susceptibility (88). PRRT2 mt increased intrinsic excitability of PyNs, and PRRT2 expression decreased sodium currents by Na$_v$1.2/Na$_v$1.6, but not Na$_v$1.1 in HEK293 cells (89). Therefore, the reduced excitability of PVINs by Nae1 deficiency is unlikely to be due to reduced levels of GABRD or PRRT2. $K^+/Cl^-$ cotransporter 2 (KCC2, encoded by *Slc12a5*) is a potassium-chloride cotransporter for maintaining the intracellular concentration of chloride ions (90). Its deficiency has been implicated in epileptogenesis (91, 92). As shown in Figure 7F, KCC2 levels were increased in Nae1-deficient mice compared with those in control samples, suggesting that the cause of epilepsy by Nae1 mutation could be complex and may involve KCC2 in addition to reduced levels of Na$_v$1.1 (see Discussion).

Note that of 53 ion channels and 29 epilepsy-associated genes, 12 were identified in both groups (Figure 7G). Only Na$_v$1.1 was reduced in *PV-Nae1$^{-/-}$-Ai9* compared with control samples. The results from proteomic analysis provide further evidence for a role of neddylation for Na$_v$1.1 stability.

*Restoring the excitability of Nae1 mt PVINs by expressing Na$_v$1.1.* Our hypothesis was that Nae1 deficiency reduces Na$_v$1.1 and thus the excitability of PVINs, which causes epilepsy. To further test this, we determined whether expressing Na$_v$1.1 in Nae1 mt PVINs

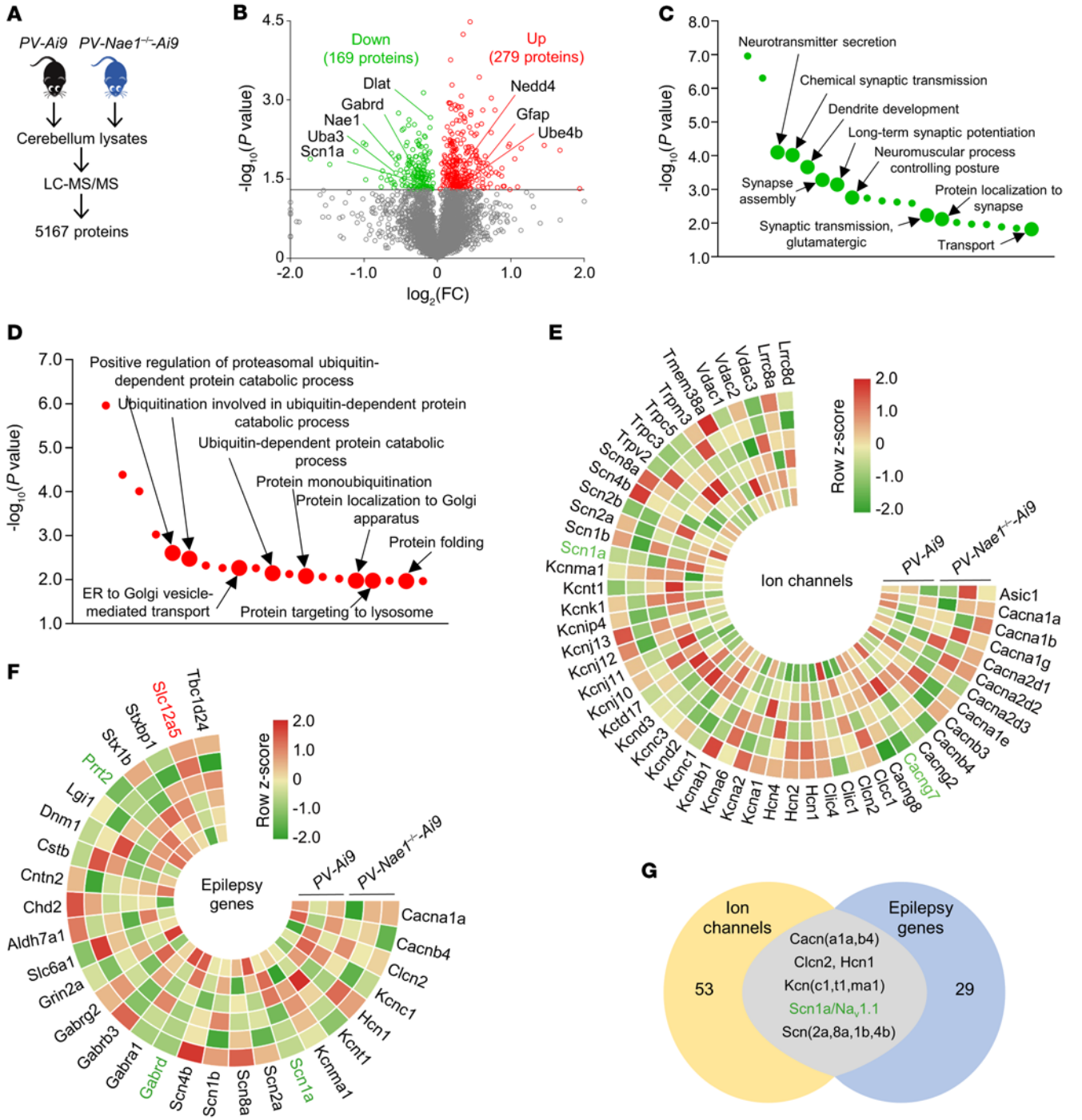


**Figure 7. Proteomic analysis revealed reduced $Na_v1.1$ and compromised synaptic function and metabolic pathways in *PV-Nae1*–deficient mice.** (**A**) Schematic diagram of quantitative proteomic analysis in *PV-Ai9* and *PV-Nae1*$^{-/-}$*-Ai9* mice. $n$ = 3 mice per genotype. (**B**) Volcano plots of differentially expressed proteins in *PV-Nae1*$^{-/-}$*-Ai9* mice over *PV-Ai9* mice. Green and red dots indicate significantly down- and upregulated proteins, respectively. (**C**) Top 20 significantly enriched GO terms of downregulated proteins. (**D**) Top 20 significantly enriched GO terms of upregulated proteins. (**E**) Heatmap of ion channel proteins. Green, downregulated ion channels. (**F**) Heatmap of proteins associated with epilepsy. Green and red colors indicate down- and upregulated proteins, respectively. (**G**) Twelve ion channels were epilepsy-associated genes, but only $Na_v1.1$ was significantly reduced by Nae1 mutation.

ameliorates the impact of Nae1 mutation on the excitability. LSL-GFP and $hNa_v1.1$-Myc plasmids were injected into the cortex of *PV-Nae1*$^{-/-}$*-Ai9* mice (Figure 8A and ref. 93). Expression of GFP was dependent on Cre. As shown in Figure 8B, GFP and $hNa_v1.1$-Myc were detected specifically in PVINs that were labeled by tdTomato in *PV-Nae1*$^{-/-}$*-Ai9* mice. First, we determined whether $hNa_v1.1$ expression increased somatic $Na^+$ currents in $GFP^+$ INs. Voltage-clamp step recording showed that the $Na_v$ current density was lower in LSL-GFP–injected *PV-Nae1*$^{-/-}$*-Ai9* mice compared with LSL-GFP–injected *PV-Ai9* mice; however, the $Na_v$ current density in mt mice injected

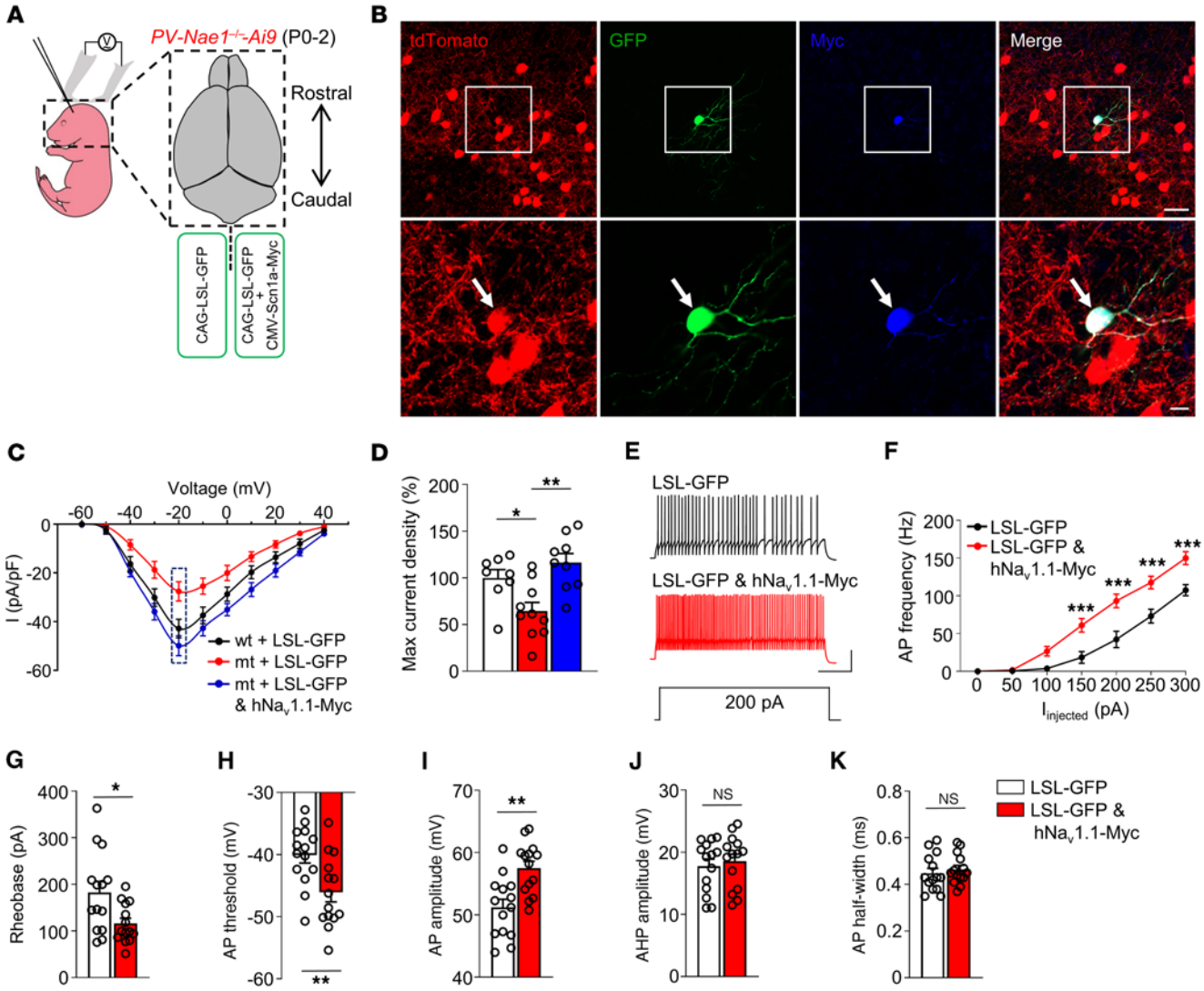


**Figure 8. Restoration of Nae1 mt PVIN excitability by expressing $Na_v1.1$.** (**A**) A diagram of in vivo electroporation. (**B**) Expression of $hNa_v1.1$-Myc and GFP in PVINs. GFP (green) signaling colocalized with anti-Myc (blue). White arrows indicate PVINs. $n$ = 3 experiments. Scale bars: 40 μm (top row); 10 μm (bottom row). (**C**) Current-voltage curves of sodium-current density in $GFP^+$ neurons. $n$ = 8–10 neurons, 5 mice for each genotype. (**D**) Rescue of sodium-current density by $Na_v1.1$ expression in *PV-Nae1*–deficient mice. (**E** and **F**) Increased excitability of mt PVINs after expressing $Na_v1.1$. Representative AP traces and quantification of current injection-induced APs in $GFP^+$ IN. $n$ = 10–11 neurons, 5 mice for each group. Scale bar: 0.2 s, 30 mV. (**G**–**K**) Rescue of AP deficits of PVINs by $Na_v1.1$ expression in *PV-Nae1* deficient mice. Decreased rheobase (**G**) and AP threshold (**H**). Increased AP amplitude (**I**). No effect on AHP amplitude (**J**) and AP half-width (**K**). $n$ = 14 neurons, 5 mice for each group. Data are represented as mean ± SEM. $^*P < 0.05$; $^{**}P < 0.01$, 1-way ANOVA (**D**); 2-way ANOVA (**F**); unpaired 2-tailed Student's $t$ test (**G**, **H**, **I**, **J**, and **K**).

with LSL-GFP and $hNa_v1.1$-Myc was increased to a level comparable to that of control mice (Figure 8, C and D, max current density 100% ± 8.92% in wt + LSL-GFP versus 64.4% ± 9.30% in mt + LSL-GFP, $P < 0.05$; 116.4% ± 9.66% in mt + LSL-GFP & $hNa_v1.1$-Myc versus 64.4% ± 9.30% in mt + LSL-GFP, $P < 0.01$; $n$ = 8–10 neurons from 4 mice per group). Next, we analyzed the intrinsic excitability, rheobase, and single AP properties of $GFP^+$ INs in *PV-Nae1*$^{-/-}$*-Ai9* mice. Compared with PVINs expressing LSL-GFP, neurons expressing $hNa_v1.1$-Myc generated more APs in response to injected currents, indicative of improved excitability (Figure 8, E and F; expression effect, $F_{1,133} = 61.8$, $P < 0.0001$; interaction effect, $F_{6,133} = 4.71$, $P < 0.001$; 2-way ANOVA). $Na_v1.1$ expression also decreased AP rheobases (Figure 8G; 116.2 ± 11.2 pA in $hNa_v1.1$ versus 182.7 ± 23.1 pA in control, $P < 0.05$; $n$ = 14 neurons from 5 mice per genotype) and thresholds (Figure 8H; −46.1 ± 1.53 mV in $hNa_v1.1$ versus −40.1 ± 1.29 mV in control, $P < 0.01$) and increased AP amplitudes (Figure 8I; 57.5 ± 1.11 mV in $hNa_v1.1$ versus 51.2 ± 1.30 mV in control, $P < 0.01$), but had no effect on AHP amplitudes and AP half-widths (Figure 8, J and K; AHP amplitude, 18.5 ± 1.14 mV in $hNa_v1.1$ versus 17.8 ± 1.11 mV in control, $P = 0.6348$; AP half-width, 0.47 ± 0.02 ms in $hNa_v1.1$ versus 0.45 ± 0.02 ms in control, $P = 0.5489$). These findings demonstrate that restoring $hNa_v1.1$ in neddylation-deficient PVINs was sufficient to recover the excitability, suggesting that $Na_v1.1$ deficiency is a major mechanism of Nae1 mutation in regulating PVIN excitability. Taken together, these results indicate that $Na_v1.1$ requires neddylation for stable expression in PVINs and thus their excitability.

## Discussion

In the present study, we uncovered a previously unknown mechanism for regulating the intrinsic excitability of PVINs. Loss of the obligatory subunit of neddylation E1, NAE1, reduced the intrinsic excitability of PVINs, but had little effect on their RMP, $C_m$, and $R_{in}$. As a result, AP thresholds were increased and amplitudes were reduced. Ensuing reduced GABA transmission and E-I imbalance resulted in spontaneous epileptic seizures. These results reveal a critical role of neddylation in regulating the excitability of INs. Further mechanistic studies identified $Na_v1.1$ as a major target for Nae1 mutation because voltage-clamp step recording indicated that Nae1 mutation reduced the Na-current density without changing its voltage dependence. In accordance with this, WB revealed lower levels of the $Na_v1.1$ protein in Nae1 mt mice or cells where neddylation was pharmacologically inhibited. This idea was supported by proteomic analysis, which also revealed abnormalities in synapses and metabolic pathways (see below). Finally, $Na_v1.1$ expression restored the excitability in PVINs in Nae1 mt mice. These results demonstrate that neddylation is necessary for the stability of $Na_v1.1$ in PVINs, revealing what we believe is a new regulatory mechanism for the excitability of INs.

Implicated in gene transcription and proteolysis, neddylation regulates cell division, differentiation, and apoptosis (33–35). Nae1 mutation in developing brain (via Emx1-Cre) impairs cortical lamination and in adult PyNs (via CaMKII-CreER) reduces spine numbers, suppresses evoked excitatory postsynaptic potential, and impairs learning and memory in mt mice (37, 94). Rapsyn, a classic adaptor protein, possesses E3 ligase activity that regulates acetylcholine receptor clustering and neuromuscular junction formation (36, 95). Here, we show that PVIN-specific mutation of Nae1 causes epilepsy and reduces the intrinsic excitability of PVINs, but has no apparent effects on that of PyNs (Figure 1C and Figure 3). No significant changes in mRNA and protein levels were observed for proteins known to regulate the excitability of PVINs, including HCN4 and voltage-gated potassium channels (Figure 7E and Supplemental Figure 7A). Among the α subunits of voltage-gated sodium channels that are critical to PVIN excitability, only $Na_v1.1$ was reduced by WB analysis and nonbiased proteomic analysis (Figure 4M and Figure 7E). In agreement, first, AP thresholds and amplitudes, both requiring sodium channels, were increased and decreased, respectively (Figure 4, D and E). Second, the $Na_v$ current density was reduced in *PV-Nae1*$^{-/-}$*-Ai9* mice compared with control mice (Figure 4, I and J). However, the Nae1 mutation had little effect on voltage-gated calcium channels and hyperpolarization-activated cyclic nucleotide-gated channels in PVINs (Supplemental Figure 7, B–F). Third, epileptic and electrophysiological phenotypes were similar between *PV-Nae1*$^{-/-}$*-Ai9* mice and $Na_v1.1$ heterozygous mt mice (7, 12, 16, 23, 41). Finally, in vivo expression of $Na_v1.1$ increased the intrinsic excitability of PVINs, reduced AP thresholds, and increased AP amplitudes (Figure 8, H and I). A parsimonious interpretation of these results is that neddylation is critical to PVIN intrinsic excitability, acting by maintaining $Na_v1.1$ stability. In support of this notion, proteomic analysis and RT-PCR failed to detect changes in proteins that regulate sodium-channel levels and functions, including auxiliary β subunits of sodium channels, FGF14, NEDD4L, and RACK1 (Supplemental Figure 11).

Mutations or loss of function in $Na_v1.1$ causes a spectrum of epileptic syndromes such as SMEI and GEFS$^+$. T875M and R1648H were the first missense mutations identified in patients with GEFS$^+$ (20), and L986F was initially identified in SEMI (21). Since then, more dysfunctional mutations have been identified and have appeared to have different pathological mechanisms. For example, T875M and W1204R mutations exhibited depolarizing and hyperpolarizing shifts of channel activation, respectively (70). The R1657C mutation reduced current density, depolarizing shift of channel activation and fast recovery of slow inactivation (96). Besides the biophysical properties, mutations R1648C and G1674R may impair intracellular trafficking and reduce surface expression (28). The D1866Y mutation was reported to disrupt the interaction between $Na_v1.1$ and the $\beta_1$ subunit, altering the voltage dependence and kinetics (97). Our study shows that the K1936E mutation could reduce $Na_v1.1$ surface expression by impairing its neddylation. In agreement with this, K48-linked ubiquitination was increased in *PV-Nae1*$^{-/-}$*-Ai9* mice compared with *PV-Ai9* mice, suggesting that neddylation could increase $Na_v1.1$'s stability by inhibiting ubiquitination. Our study thus provides what we believe is a previously unknown pathological mechanism of $Na_v1.1$ mutations. The K245N mutation, located within the cytosolic S4-S5 linker of domain I in $Na_v1.1$ (65), may act in a pathogenic way by decreasing fast inactivation of sodium channels without altering neddylation.

The E-I balance is not only controlled by the intrinsic excitability of PVINs, but also that of CCKINs, a major source of inhibitory signals that has been implicated in epilepsy (98). On the other hand, astrocytes could modulate the neuronal activity by altering extracellular concentrations of ATP, potassium, and glutamate and thus epileptogenesis (99–102). However, Nae1 mutation in PVINs had little effect on CCKIN intrinsic excitability and astrocytic electrophysiological properties (Supplemental Figure 5). Proteomic analysis indicates that, of the currently known 29 epilepsy-associated risk genes, in addition to $Na_v1.1$, GABRD and PRRT2 were reduced (Figure 7F). However, IN-specific deletion GABRD increased IN excitability, as described earlier (88). PRRT2 mt mice displayed increased intrinsic excitability of PyNs (89), which was not observed in Nae1 mt mice. Moreover, PRRT2 coexpression had little effect on $Na_v1.1$ in HEK293 cells (89). However, global GABRD knockout decreased inhibition onto granule cells and thus increased seizure susceptibility (103); PRRT2 reduction in PyNs was shown to increase the excitability of PyNs by increasing sodium-channel currents (89) and is thus likely to cause epilepsy. These suggest that the pathological mechanisms of epilepsy may be complex and may involve reduced GABRD and PRRT2 in other cells. Because Nae1 was ablated specifically in PVINs, these effects may be secondary. In addition, proteomic analysis also revealed an increase in KCC2 in *PV-Nae1*$^{-/-}$*-Ai9* mice compared with controls (Figure 7F). Low levels of KCC2 enable GABA to be excitatory in PyNs, whereas increased KCC2 in PyNs renders GABA to be inhibitory (104). These observations suggest that KCC2 increase may result from a compensatory mechanism.

Interestingly, GO and KEGG analyses of Nae1 mutation–downregulated proteins highlighted functional processes, such as dendrite development, synapse organization, synaptic vesicle exocytosis, glutamatergic transmission, dopaminergic synapses, endocannabinoid signaling, and alcoholism as well as spliceosome (Figure 7C and Supplemental Figure 12A, and Supplemental Tables 2 and 3). On the other hand, analysis of the upregulated

proteins suggested changes in ubiquitin-regulated catabolism, protein folding and localization, and metabolic pathways, including propanoate, pyruvate and carbon metabolism, tRNA synthesis, phagocytosis, and ubiquitin-mediated proteolysis (Figure 7D, Supplemental Figure 12B, and Supplemental Tables 4 and 5). Determining whether these processes contribute to epileptogenesis warrants future studies. Our study identifies a regulatory mechanism of $Na_v1.1$ stability in PVINs by neddylation and demonstrates that deficient neddylation reduces $Na_v1.1$ levels, which reduces the excitability of PVINs and thus epilepsy. Increasing Scn1a expression could elevate the excitability of Scn1a-deficient PVINs and attenuate epileptic phenotypes in Dravet syndrome mouse models (105). Selective activators of $Na_v1.1$ also benefit seizure (106) and other $Na_v1.1$-associated deficits (107). Further studies are necessary to explore whether modification of neddylation represents a new therapeutic strategy for epilepsy.

## Methods

Detailed methods are provided in Supplemental Methods.

*Statistics*. Data were analyzed with GraphPad Prism software. For analysis between 2 groups, 2-tailed unpaired Student's *t* test was used. For analysis of multiple groups at single time points, 1-way ANOVA was used, followed by Tukey-Kramer post hoc multiple comparisons test. For analysis of multiple groups at multiple time points, 2-way ANOVA was used, followed by Bonferroni's post hoc multiple comparisons test. Data were expressed as mean ± SEM. $P < 0.05$ was considered statistically significant.

*Study approval*. These studies were approved by the Institutional Animal Care and Use Committee of Augusta University and Case Western Reserve University.

## Author contributions

W Chen, WCX, and LM designed research studies. W Chen, BL, NG, HL, HW, LL, W Cui, LZ, DS, FL, ZD, XR, and HZ performed experiments and analyzed data. HS provided material support and discussion. W Chen and LM wrote the manuscript.

## Acknowledgments

We thank Qing K. Wang (Cleveland Clinic, Cleveland, Ohio, USA) for the generous supply of tsA-201 cells. We also thank Guanglin Xing, Zhibing Tan, Kai Zhao, and Xiangdong Sun for kind suggestions. We thank Piliang Hao and Chengqian Zhang for assistance with mass spectrometry equipment at the Biological Mass Spectrometry Core Facility, ShanghaiTech University. This work was supported by a startup grant from Case Western Reserve University.

Address correspondence to: Lin Mei, Department of Neurosciences, School of Medicine, Case Western Reserve University, 10900 Euclid Avenue, Cleveland, Ohio, USA. Phone: 216.368.4928; Email: lin.mei@case.edu.

1. Bartos M, et al. Synaptic mechanisms of synchronized gamma oscillations in inhibitory interneuron networks. *Nat Rev Neurosci*. 2007;8(1):45–56.
2. Cardin JA, et al. Driving fast-spiking cells induces gamma rhythm and controls sensory responses. *Nature*. 2009;459(7247):663–667.
3. Sohal VS, et al. Parvalbumin neurons and gamma rhythms enhance cortical circuit performance. *Nature*. 2009;459(7247):698–702.
4. Donato F, et al. Parvalbumin-expressing basket-cell network plasticity induced by experience regulates adult learning. *Nature*. 2013;504(7479):272–276.
5. Hensch TK. Critical period plasticity in local cortical circuits. *Nat Rev Neurosci*. 2005;6(11):877–888.
6. Hu H, et al. Interneurons. Fast-spiking, parvalbumin$^+$ GABAergic interneurons: from cellular design to microcircuit function. *Science*. 2014;345(6196):1255263.
7. Ogiwara I, et al. Nav1.1 localizes to axons of parvalbumin-positive inhibitory interneurons: a circuit basis for epileptic seizures in mice carrying an Scn1a gene mutation. *J Neurosci*. 2007;27(22):5903–5914.
8. Rubinstein M, et al. Dissecting the phenotypes of Dravet syndrome by gene deletion. *Brain*. 2015;138(Pt 8):2219–2233.
9. Wang W, et al. The developmental changes of Na(v)1.1 and Na(v)1.2 expression in the human hippocampus and temporal lobe. *Brain Res*. 2011;1389:61–70.
10. Tian C, et al. Molecular identity of axonal sodium channels in human cortical pyramidal cells. *Front Cell Neurosci*. 2014;8:297.
11. Lorincz A, Nusser Z. Cell-type-dependent molecular composition of the axon initial segment. *J Neurosci*. 2008;28(53):14329–14340.
12. Frank HY, et al. Reduced sodium current in GABAergic interneurons in a mouse model of severe myoclonic epilepsy in infancy. *Nat Neurosci*. 2006;9(9):1142–1149.
13. Verret L, et al. Inhibitory interneuron deficit links altered network activity and cognitive dysfunction in Alzheimer model. *Cell*. 2012;149(3):708–721.
14. Hedrich UB, et al. Impaired action potential initiation in GABAergic interneurons causes hyperexcitable networks in an epileptic mouse model carrying a human Na(V)1.1 mutation. *J Neurosci*. 2014;34(45):14874–14889.
15. De Stasi AM, et al. Unaltered network activity and interneuronal firing during spontaneous cortical dynamics in vivo in a mouse model of severe myoclonic epilepsy of infancy. *Cereb Cortex*. 2016;26(4):1778–1794.
16. Tai C, et al. Impaired excitability of somatostatin- and parvalbumin-expressing cortical interneurons in a mouse model of Dravet syndrome. *Proc Natl Acad Sci U S A*. 2014;111(30):E3139–E3148.
17. Lau D, et al. Impaired fast-spiking, suppressed cortical inhibition, and increased susceptibility to seizures in mice lacking Kv3.2 K+ channel proteins. *J Neurosci*. 2000;20(24):9071–9085.
18. Espinosa F, et al. Ablation of Kv3.1 and Kv3.3 potassium channels disrupts thalamocortical oscillations in vitro and in vivo. *J Neurosci*. 2008;28(21):5570–5581.
19. Soh H, et al. Deletion of KCNQ2/3 potassium channels from PV+ interneurons leads to homeostatic potentiation of excitatory transmission. *Elife*. 2018;7:e38617.
20. Escayg A, et al. Mutations of SCN1A, encoding a neuronal sodium channel, in two families with GEFS+2. *Nat Genet*. 2000;24(4):343–345.
21. Claes L, et al. De novo mutations in the sodium-channel gene SCN1A cause severe myoclonic epilepsy of infancy. *Am J Hum Genet*. 2001;68(6):1327–1332.
22. Wallace RH, et al. Neuronal sodium-channel alpha1-subunit mutations in generalized epilepsy with febrile seizures plus. *Am J Hum Genet*. 2001;68(4):859–865.
23. Tang B, et al. A BAC transgenic mouse model reveals neuron subtype-specific effects of a generalized epilepsy with febrile seizures plus (GEFS+) mutation. *Neurobiol Dis*. 2009;35(1):91–102.
24. Martin MS, et al. Altered function of the SCN1A voltage-gated sodium channel leads to gamma-aminobutyric acid-ergic (GABAergic) interneuron abnormalities. *J Biol Chem*. 2010;285(13):9823–9834.
25. Cheah CS, et al. Specific deletion of NaV1.1 sodium channels in inhibitory interneurons causes seizures and premature death in a mouse model of Dravet syndrome. *Proc Natl Acad Sci U S A*. 2012;109(36):14646–14651.
26. Catterall WA, et al. NaV1.1 channels and epilepsy. *J Physiol*. 2010;588(Pt 11):1849–1859.
27. Patino GA, et al. A functional null mutation of SCN1B in a patient with Dravet syndrome. *J Neurosci*. 2009;29(34):10764–10778.
28. Thompson CH, et al. Nontruncating SCN1A mutations associated with severe myoclonic epilepsy of infancy impair cell surface expression. *J Biol Chem*. 2012;287(50):42001–42008.
29. Hochstrasser M. Origin and function of ubiquitin-like proteins. *Nature*. 2009;458(7237):422–429.
30. Gan-Erdene T, et al. Identification and characterization of DEN1, a deneddylase of the ULP family. *J Biol Chem*. 2003;278(31):28892–28900.
31. Kamitani T, et al. Characterization of NEDD8,

a developmentally down-regulated ubiquitin-like protein. *J Biol Chem*. 1997;272(45):28557–28562.
32. Menon S, et al. COP9 signalosome subunit 8 is essential for peripheral T cell homeostasis and antigen receptor-induced entry into the cell cycle from quiescence. *Nat Immunol*. 2007;8(11):1236–1245.
33. Rabut G, Peter M. Function and regulation of protein neddylation. 'Protein modifications: beyond the usual suspects' review series. *EMBO Rep*. 2008;9(10):969–976.
34. Enchev RI, et al. Protein neddylation: beyond cullin-RING ligases. *Nat Rev Mol Cell Biol*. 2015;16(1):30–44.
35. Kandala S, et al. Neddylation and deneddylation in cardiac biology. *Am J Cardiovasc Dis*. 2014;4(4):140–158.
36. Li L, et al. Enzymatic activity of the scaffold protein rapsyn for synapse formation. *Neuron*. 2016;92(5):1007–1019.
37. Vogl AM, et al. Neddylation inhibition impairs spine development, destabilizes synapses and deteriorates cognition. *Nat Neurosci*. 2015;18(2):239–251.
38. Zou J, et al. Neddylation mediates ventricular chamber maturation through repression of Hippo signaling. *Proc Natl Acad Sci U S A*. 2018;115(17):E4101–E4110.
39. Hippenmeyer S, et al. A developmental switch in the response of DRG neurons to ETS transcription factor signaling. *PLoS Biol*. 2005;3(5):e159.
40. Madisen L, et al. A robust and high-throughput Cre reporting and characterization system for the whole mouse brain. *Nat Neurosci*. 2010;13(1):133–140.
41. Kalume F, et al. Reduced sodium current in Purkinje neurons from Nav1.1 mutant mice: implications for ataxia in severe myoclonic epilepsy in infancy. *J Neurosci*. 2007;27(41):11065–11074.
42. Favuzzi E, et al. Activity-Dependent Gating of Parvalbumin Interneuron Function by the Perineuronal Net Protein Brevican. *Neuron*. 2017;95(3):639–655.
43. Dehorter N, et al. Tuning of fast-spiking interneuron properties by an activity-dependent transcriptional switch. *Science*. 2015;349(6253):1216–1220.
44. Hughes DI, et al. HCN4 subunit expression in fast-spiking interneurons of the rat spinal cord and hippocampus. *Neuroscience*. 2013;237:7–18.
45. Li T, et al. Action potential initiation in neocortical inhibitory interneurons. *PLoS Biol*. 2014;12(9):e1001944.
46. Rudy B, McBain CJ. Kv3 channels: voltage-gated K+ channels designed for high-frequency repetitive firing. *Trends Neurosci*. 2001;24(9):517–526.
47. Erisir A, et al. Function of specific K(+) channels in sustained high-frequency firing of fast-spiking neocortical interneurons. *J Neurophysiol*. 1999;82(5):2476–2489.
48. Colbert CM, Pan E. Ion channel properties underlying axonal action potential initiation in pyramidal neurons. *Nat Neurosci*. 2002;5(6):533–538.
49. Kole MH, et al. Action potential generation requires a high sodium channel density in the axon initial segment. *Nat Neurosci*. 2008;11(2):178–186.
50. Hodgkin AL, Huxley AF. A quantitative description of membrane current and its application to conduction and excitation in nerve. *J Physiol*. 1952;117(4):500–544.
51. Bean BP. The action potential in mammalian central neurons. *Nat Rev Neurosci*. 2007;8(6):451–465.
52. Aldrich RW Jr, et al. Mechanism of frequency-dependent broadening of molluscan neurone soma spikes. *J Physiol*. 1979;291:531–544.
53. Shao LR, et al. The role of BK-type Ca2+-dependent K+ channels in spike broadening during repetitive firing in rat hippocampal pyramidal cells. *J Physiol*. 1999;521 Pt 1:135–146.
54. Milescu LS, et al. Isolation of somatic Na+ currents by selective inactivation of axonal channels with a voltage prepulse. *J Neurosci*. 2010;30(22):7740–7748.
55. Yamagata T, et al. Nav1.2 is expressed in caudal ganglionic eminence-derived disinhibitory interneurons: mutually exclusive distributions of Nav1.1 and Nav1.2. *Biochem Biophys Res Commun*. 2017;491(4):1070–1076.
56. Zhao Y, et al. Targeting Neddylation pathways to inactivate cullin-RING ligases for anticancer therapy. *Antioxid Redox Signal*. 2014;21(17):2383–2400.
57. Xirodimas DP, et al. Mdm2-mediated NEDD8 conjugation of p53 inhibits its transcriptional activity. *Cell*. 2004;118(1):83–97.
58. Ryu JH, et al. Hypoxia-inducible factor α subunit stabilization by NEDD8 conjugation is reactive oxygen species-dependent. *J Biol Chem*. 2011;286(9):6963–6970.
59. Tapper AR, et al. Heterologous expression of ion channels. *Methods Mol Biol*. 2003;217:285–294.
60. Brownell JE, et al. Substrate-assisted inhibition of ubiquitin-like protein-activating enzymes: the NEDD8 E1 inhibitor MLN4924 forms a NEDD8-AMP mimetic in situ. *Mol Cell*. 2010;37(1):102–111.
61. Soucy TA, et al. An inhibitor of NEDD8-activating enzyme as a new approach to treat cancer. *Nature*. 2009;458(7239):732–736.
62. Watson IR, et al. Mdm2-mediated NEDD8 modification of TAp73 regulates its transactivation function. *J Biol Chem*. 2006;281(45):34096–34103.
63. Xu X, et al. Amplicon resequencing identified parental mosaicism for approximately 10% of "de novo" SCN1A mutations in children with Dravet syndrome. *Hum Mutat*. 2015;36(9):861–872.
64. Lee HF, et al. Electroencephalographic features of patients with SCN1A-positive Dravet syndrome. *Brain Dev*. 2015;37(6):599–611.
65. Morimoto M, et al. SCN1A mutation mosaicism in a family with severe myoclonic epilepsy in infancy. *Epilepsia*. 2006;47(10):1732–1736.
66. Orrico A, et al. Mutational analysis of the SCN1A, SCN1B and GABRG2 genes in 150 Italian patients with idiopathic childhood epilepsies. *Clin Genet*. 2009;75(6):579–581.
67. Abou-Khalil B, et al. Partial and generalized epilepsy with febrile seizures plus and a novel SCN1A mutation. *Neurology*. 2001;57(12):2265–2272.
68. Lindy AS, et al. Diagnostic outcomes for genetic testing of 70 genes in 8565 patients with epilepsy and neurodevelopmental disorders. *Epilepsia*. 2018;59(5):1062–1071.
69. Goldberg-Stern H, et al. Broad phenotypic heterogeneity due to a novel SCN1A mutation in a family with genetic epilepsy with febrile seizures plus. *J Child Neurol*. 2014;29(2):221–226.
70. Lossin C, et al. Molecular basis of an inherited epilepsy. *Neuron*. 2002;34(6):877–884.
71. Casini S, et al. Intracellular calcium modulation of voltage-gated sodium channels in ventricular myocytes. *Cardiovasc Res*. 2009;81(1):72–81.
72. Isom LL, et al. Primary structure and functional expression of the beta 1 subunit of the rat brain sodium channel. *Science*. 1992;256(5058):839–842.
73. Isom LL, et al. Structure and function of the beta 2 subunit of brain sodium channels, a transmembrane glycoprotein with a CAM motif. *Cell*. 1995;83(3):433–442.
74. Lou JY, et al. Fibroblast growth factor 14 is an intracellular modulator of voltage-gated sodium channels. *J Physiol*. 2005;569(Pt 1):179–193.
75. Laezza F, et al. FGF14 N-terminal splice variants differentially modulate Nav1.2 and Nav1.6-encoded sodium channels. *Mol Cell Neurosci*. 2009;42(2):90–101.
76. Shakkottai VG, et al. FGF14 regulates the intrinsic excitability of cerebellar Purkinje neurons. *Neurobiol Dis*. 2009;33(1):81–88.
77. Rougier JS, et al. Molecular determinants of voltage-gated sodium channel regulation by the Nedd4/Nedd4-like proteins. *Am J Physiol Cell Physiol*. 2005;288(3):C692–C701.
78. van Bemmelen MX, et al. Cardiac voltage-gated sodium channel Nav1.5 is regulated by Nedd4-2 mediated ubiquitination. *Circ Res*. 2004;95(3):284–291.
79. Abriel H, et al. Regulation of the cardiac voltage-gated Na+ channel (H1) by the ubiquitin-protein ligase Nedd4. *FEBS Lett*. 2000;466(2–3):377–380.
80. Dong ZF, et al. Transcription of the human sodium channel SCN1A gene is repressed by a scaffolding protein RACK1. *Mol Neurobiol*. 2014;50(2):438–448.
81. Yamazaki M, et al. TARPs gamma-2 and gamma-7 are essential for AMPA receptor expression in the cerebellum. *Eur J Neurosci*. 2010;31(12):2204–2220.
82. Yamazaki M, et al. Relative contribution of TARPs γ-2 and γ-7 to cerebellar excitatory synaptic transmission and motor behavior. *Proc Natl Acad Sci U S A*. 2015;112(4):E371–E379.
83. Heron SE, et al. PRRT2 mutations cause benign familial infantile epilepsy and infantile convulsions with choreoathetosis syndrome. *Am J Hum Genet*. 2012;90(1):152–160.
84. Dibbens LM, et al. GABRD encoding a protein for extra- or peri-synaptic GABAA receptors is a susceptibility locus for generalized epilepsies. *Hum Mol Gene*t. 2004;13(13):1315–1319.
85. Stodberg T, et al. Mutations in SLC12A5 in epilepsy of infancy with migrating focal seizures. *Nat Commun*. 2015;6:8038.
86. Cossette P, et al. Mutation of GABRA1 in an autosomal dominant form of juvenile myoclonic epilepsy. *Nat Genet*. 2002;31(2):184–189.
87. Heron SE, et al. Sodium-channel defects in benign familial neonatal-infantile seizures. *Lancet*. 2002;360(9336):851–852.
88. Lee V, Maguire J. Impact of inhibitory constraint of interneurons on neuronal excitability. *J Neurophysiol*. 2013;110(11):2520–2535.
89. Fruscione F, et al. PRRT2 controls neuronal excitability by negatively modulating Na+ channel 1.2/1.6 activity. *Brain*. 2018;141(4):1000–1016.
90. Kaila K, et al. Cation-chloride cotransporters in neuronal development, plasticity and disease. *Nat Rev Neurosci*. 2014;15(10):637–654.
91. Woo NS, et al. Hyperexcitability and epilepsy

associated with disruption of the mouse neuronal-specific K-Cl cotransporter gene. *Hippocampus*. 2002;12(2):258–268.
92. Tornberg J, et al. Behavioural phenotypes of hypomorphic KCC2-deficient mice. *Eur J Neurosci*. 2005;21(5):1327–1337.
93. Jiao HF, et al. Transmembrane protein 108 is required for glutamatergic transmission in dentate gyrus. *Proc Natl Acad Sci U S A*. 2017;114(5):1177–1182.
94. Zhang L, et al. Neddylation is critical to cortical development by regulating Wnt/β-catenin signaling. *Proc Natl Acad Sci U S A*. 2020;117(42):26448–26459.
95. Xing G, et al. A mechanism in agrin signaling revealed by a prevalent Rapsyn mutation in congenital myasthenic syndrome. *Elife*. 2019;8:e49180.
96. Lossin C, et al. Epilepsy-associated dysfunction in the voltage-gated neuronal sodium channel SCN1A. *J Neurosci*. 2003;23(36):11289–11295.
97. Spampanato J, et al. A novel epilepsy mutation in the sodium channel SCN1A identifies a cytoplasmic domain for beta subunit interaction. *J Neurosci*. 2004;24(44):10022–10034.
98. Wyeth MS, et al. Selective reduction of cholecystokinin-positive basket cell innervation in a model of temporal lobe epilepsy. *J Neurosci*. 2010;30(26):8993–9006.
99. Patel DC, et al. Neuron-glia interactions in the pathophysiology of epilepsy. *Nat Rev Neurosci*. 2019;20(5):282–297.
100. Djukic B, et al. Conditional knock-out of Kir4.1 leads to glial membrane depolarization, inhibition of potassium and glutamate uptake, and enhanced short-term synaptic potentiation. *J Neurosci*. 2007;27(42):11354–11365.
101. Steinhauser C, et al. Astrocyte dysfunction in temporal lobe epilepsy: K+ channels and gap junction coupling. *Glia*. 2012;60(8):1192–1202.
102. Sun XD, et al. Lrp4 in astrocytes modulates glutamatergic transmission. *Nat Neurosci*. 2016;19(8):1010–1018.
103. Spigelman I, et al. Reduced inhibition and sensitivity to neurosteroids in hippocampus of mice lacking the GABA(A) receptor delta subunit. *J Neurophysiol*. 2003;90(2):903–910.
104. Moore YE, et al. Seizing control of KCC2: a new therapeutic target for epilepsy. *Trends Neurosci*. 2017;40(9):555–571.
105. Colasante G, et al. dCas9-based Scn1a gene activation restores inhibitory interneuron excitability and attenuates seizures in Dravet Syndrome mice. *Mol Ther*. 2020;28(1):235–253.
106. Richards KL, et al. Selective $Na_V1.1$ activation rescues Dravet syndrome mice from seizures and premature death. *Proc Natl Acad Sci U S A*. 2018;115(34):E8077–E8085.
107. Jensen HS, et al. Therapeutic potential of Na(V)1.1 activators. *Trends Pharmacol Sci*. 2014;35(3):113–118.